Physics – Uspekhi **53** (9) 933 – 961 (2010)

CONFERENCES AND SYMPOSIA

PACS number: 01.10.Fv, **07.87.+v**, 52.30.Cv, 52.35.Py, 52.35.Vd, 96.50.S–, 96.60.Q–, **96.60.–j**, 96.60.qe, 97.60.Bw, 98.62.Nx

Commemoration of the 85th birthday of S I Syrovatskii (Scientific session of the Physical Sciences Division of the Russian Academy of Sciences, 26 May 2010)

DOI: 10.3367/UFNe.0180.201009f.0973

A scientific session of the Physical Sciences Division, Russian Academy of Sciences (RAS), was held on 26 May 2010 at the conference hall of the Lebedev Physical Institute, RAS. The session was devoted to the 85th birthday of S I Syrovatskii.

The program announced on the web page of the RAS Physical Sciences Division (www.gpad.ac.ru) contained the following reports:

(1) **Zelenyi L M** (Space Research Institute, RAS, Moscow) "Current sheets and reconnection in the geomagnetic tail";

(2) **Frank A G** (Prokhorov General Physics Institute, RAS, Moscow) "Dynamics of current sheets as the cause of flare events in magnetized plasmas";

(3) **Kuznetsov V D** (Pushkov Institute of Terrestrial Magnetism, the Ionosphere, and Radio Wave Propagation, RAS, Troitsk, Moscow region) "Space research on the Sun";

(4) **Somov B V** (Shternberg Astronomical Institute, Lomonosov Moscow State University, Moscow) "Strong shock waves and extreme plasma states";

(5) **Zybin K P** (Lebedev Physical Institute, RAS, Moscow) "Structure functions for developed turbulence";

(6) **Ptuskin V S** (Pushkov Institute of Terrestrial Magnetism, the Ionosphere, and Radio Wave Propagation, RAS, Troitsk, Moscow region) "The origin of cosmic rays."

Papers based on reports 1–4 and 6 are published in what follows.

Sergei Ivanovich Syrovatskii
(02.03.1925 – 26.09.1979)

PACS numbers: 52.30.Cv, 52.35.Py, 52.35.Vd
DOI: 10.3367/UFNe.0180.201009g.0973

Metastability of current sheets

L M Zelenyi, A V Artemyev, Kh V Malova, A A Petrukovich, R Nakamura

1. Introduction

A current sheet (CS) is a universal plasma structure. The formation of current sheets is observed in numerous laboratory experiments [1, Vol. 1, Ch. 9], [2, p. 108], in the solar corona [2, p. 3], [3], and in astrophysical objects (magnetospheres of stars, galactic jets, etc.) [4, 5]. They exist in the tail of Earth's magnetosphere [1, Vol. 2, Ch. 4] and at its boundary, i.e., magnetopause [6]. The presence of CSs is associated with the accumulation of magnetic field energy. Therefore, revealing the mechanisms responsible for energy accumulation in CSs without its immediate release is of great interest. Among phenomena associated with the release of the accumulated magnetic energy, we first of all note solar flares. The idea of magnetic field reconnection has been suggested in the research on the accumulated magnetic energy release by conversion to the thermal energy and the energy of particle motion in solar flares [7].

A current sheet separates two regions where magnetic field lines have opposite directions, and reconnection of these

Uspekhi Fizicheskikh Nauk **180** (9) 973 – 1004 (2004)
DOI: 10.3367/UFNr.0180.201009f.0973
Translated by V V Lobzin and S V Vladimirov;
edited by A M Semikhatov

L M Zelenyi, A A Petrukovich Space Research Institute, Russian Academy of Sciences, Moscow, Russian Federation
E-mail: lzelenyi@iki.rssi.ru
A V Artemyev, Kh V Malova Space Research Institute, Russian Academy of Sciences, Moscow, Russian Federation, Skobeltsyn Institute of Nuclear Physics, Moscow State University, Moscow, Russian Federation
R Nakamura Space Research Institute, Austrian Academy of Sciences, Graz, Austria

Uspekhi Fizicheskikh Nauk **180** (9) 973 – 982 (2010)
DOI: 10.3367/UFNr.0180.201009g.0973
Translated by V V Lobzin; edited by A M Semikhatov

lines is therefore accompanied by their disruption and the current sheet filamentation. But the first magnetic reconnection models were aimed at describing not the current sheets and their dynamics but a stationary region with the dissipation of the magnetic field (see [8] and review [9]). These models were based on the strong assumption of the existence of an equilibrium between the plasma flows incoming to the dissipation region and the fluxes of accelerated particles leaving this region. More rigorous calculations showed that the boundary conditions required for such stationary solutions in the framework of magnetohydrodynamics (MHD) cannot typically be well defined [10], and the reconnection in real problems is essentially nonstationary [11].

A more general dynamic CS formation scenario was considered by Syrovatskii [2, 12]. In solving the MHD problem of plasma flows in the vicinity of a neutral point of a magnetic field, he succeeded in developing a scenario of CS formation with a subsequent magnetic field reconnection. The finite lifetime of a CS results in the *concept of metastability*. In the framework of this concept, a CS accumulates energy during a relatively long time period, and only after that does it spontaneously release the energy during a rapid magnetic reconnection. This approach allowed explaining the alternating long-lasting periods when CSs are 'quiet' and the subsequent explosion-like releases of the accumulated energy [2, 13]; such an alternation is difficult to explain by stationary reconnection models.

Models of CSs in the solar corona and their disruption involve a mechanism of the magnetic field dissipation due to Coulomb collisions of plasma particles. Similar structures are also observed in the collisionless plasma of Earth's magnetosphere and in the solar wind. In 1965, Ness proved the existence of Earth's magnetic tail with oppositely directed magnetic fields in its northern and southern regions and a current sheet separating these regions [14]. The number density of particles in such a CS is about 1 cm^{-3}, which excludes collisional dissipation. The main mechanism responsible for the dissipation in collisionless plasmas is the kinetic effect of the resonance interaction of plasma particles with a developing unstable plasma mode in a CS (reverse Landau damping). To simulate a CS, a one-dimensional kinetic model by Harris [15] and its subsequent generalizations to the two-dimensional geometry [16, 17] are frequently used. The disruption of such a CS is related to a developing tearing instability, which was suggested in 1966 as the main candidate for the mechanism responsible for initiating the magnetic reconnection in the magnetotail [18]. Realizing the importance of kinetic effects for understanding the stability of extremely thin CSs in collisionless plasmas, Syrovatskii in cooperation with Bulanov worked out a model of the tearing instability developing in a CS of zero thickness [2, p. 88].

The transformation of the magnetic field energy into the energy of particles in collisionless plasmas is also essentially kinetic. Indeed, one of the main mechanisms of increasing the particle energy is by accelerating the particles with electric fields in the vicinity of the reconnection region. The modern theory of this process is based on the pioneering work of the Syrovatskii school [19–21], where the stationary electric field approximation was used, and the work of Galeev [22, 23], who considered the pulsed electric field approximation.

The concept of metastability was introduced in papers [24, 25] devoted to the stability theory for collisionless CSs in the magnetotail with the normal magnetic field component B_z taken into account. This component, which is nonvanishing in the CS center, magnetizes electrons and makes the field lines rigid (as if they were materialized), thereby stabilizing the tearing instability and delaying the CS filamentation. The theory of the tearing instability in Earth's magnetosphere developed in the 1970–1980s [26–29] was based on the Harris model. The above assumption was the weakest statement in the theory and then led to its abandonment (which was unjustified, as we show in what follows) as regards explaining the initialization of geomagnetic substorms (a phenomenon that is directly related to the magnetic field reconnection). In the 1990s, it was shown that the Harris CS is absolutely stable with respect to the tearing instability [30, 31]. This result favored developing alternative substorm scenarios based not on the disruption of field lines but on the disruption of current structures in the inner magnetosphere [32].

However, a growing amount of experimental data was still showing that the magnetic reconnection is the most probable mechanism of the magnetic energy transformation into the energy of particle fluxes in Earth's magnetosphere [33–35]. Moreover, using the results obtained aboard the Themis spacecraft aimed at finding substorm initialization sites, it was shown that the reconnection of field lines occurs in a region with a thin current sheet in the night-side magnetosphere at the radial distance about 16 Earth radii [36]. Thus, there was an obvious contradiction between the observational data and theoretical predictions of the absolute stability of CSs. In this paper, we discuss ways to overcome this misunderstanding regarding one of the most important phenomena in space physics.

2. Modern satellite data and theoretical models

The Syrovatskii hypothesis that thin current sheets (TCSs) play a crucial role in the accumulation and release of magnetic energy is fully confirmed by modern spacecraft data. Using the magnetic field measurements aboard two ISEE (International Sun–Earth Explorer) spacecraft, it was found that a TCS with a complicated internal structure may develop at the substorm initiation phase. A characteristic feature of such a current sheet is the distinction between the amplitude of the CS magnetic field B_0 and the field B_{ext} at the boundary of the plasma sheet. Hence, a TCS with small-scale currents is embedded into a much wider plasma sheet (the plasma of this sheet can be represented as a background of the TCS). Syrovatskii considered this model in his papers, where the background plasma was called a fur [2].

The most detailed information about CSs in Earth's magnetosphere was provided by the four-device project Cluster [38–40]. Simultaneous measurements of the magnetic field **B** at four different locations allow determining the current density $\mathbf{j} = (c/4\pi)\,\mathrm{rot}\,\mathbf{B}$ and thereby revealing the CS structure. It was found that most current sheets in the magnetotail are embedded structures [38] and cannot be described by the Harris model [40].

The embedding of CSs assumes that a small fraction of particles (10–20% of the total) creates a TCS current responsible for the magnetic field $\sim B_0$. The remaining 80–90% develop the magnetic field $B_{\mathrm{ext}} - B_0$. In this case, a typical ratio is $B_0/B_{\mathrm{ext}} \sim 0.4$ [41]. Such a CS is schematically shown in Fig. 1. Characteristic TCS scales are of the order of 1000 km, and if $B_{\mathrm{ext}} \approx 30-40$ nT, then the current density is large enough to prevent the TCS formation due

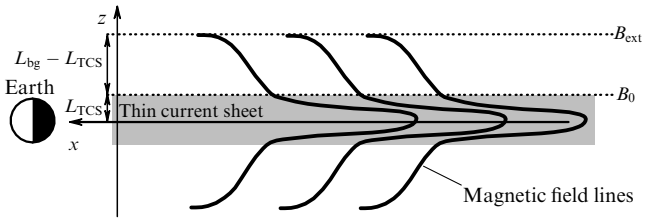

Figure 1. Schematic representation of a TCS. Shown are the thickness L_{TCS} of the current sheet and the thickness L_{bg} of the background sheet embedding the TCS. The positions corresponding to the magnetic fields B_0 and B_{ext} are also shown.

to the diamagnetic drift of plasma particles. On the other hand, it is known that transit ions with 'Speiser's trajectories' may exist in a TCS [42, 43]; because their orbits are open, such ions create a current and the projection of their flow velocities on the current direction is comparable to the thermal speed. Because the normal component of the magnetic field in a TCS is small ($B_z \ll B_0$), the ion equations of motion are integrable, and it is possible to introduce the quasiadiabatic invariant $I_z = \oint v_z \, dz$, which is conserved along the trajectories of transit particles [43]. The conservation of I_z and of the total energy H_0 allows developing a self-consistent one-dimensional model of TCSs [44, 45].

The normal component B_z of the magnetic field in the magnetotail is too small to magnetize the ions; but is large enough to regard the electrons as magnetized and to analyze their trajectories in the drift approximation. By summing the currents of the transit ions with the electron drift currents, a model of two-component TCS can be developed [46].

To write the basic equations for the one-dimensional TCS model, we choose the coordinate system shown in Fig. 1. The current is directed along the y axis; the magnetic field, which is directed along the x axis, changes its sign in the plane $z = 0$. The only spatial coordinate on which all parameters of the system depend is z. The ion distribution function at the boundary of the system can be chosen as a shifted Maxwell distribution,

$$f \sim \exp\left(-\frac{v_\perp^2 + (v_\parallel - v_D)^2}{v_T^2}\right),$$

and the main parameter of the problem is the ratio of the thermal and bulk flow velocities of ions, $\varepsilon = v_T/v_D$. In the central part of the TCS, the distribution function can be expressed in terms of the integrals of motion,

$$f \sim \exp\left[-\frac{\omega_0 I_z}{m v_T^2} - \left(\sqrt{\frac{2H_0}{m v_T^2} - \frac{\omega_0 I_z}{m v_T^2}} - \varepsilon^{-1}\right)^2\right].$$

Using the Liouville equation ($df/dt = 0$), the ion current $j_i = q_i \int v_y f \, d^3v$ can then be calculated at each point. Here, m and q_i are the ion mass and charge, and ω_0 is the ion gyrofrequency at the TCS boundary. The quasiadiabatic invariant I_z is then a nonlocal function of the magnetic field B_x:

$$I_z \sim m \oint \sqrt{v_y^2 + v_z^2 - \left(v_y - \frac{q_i}{mc}\int_{z'}^{z} B_x(z'')\,dz''\right)^2}\, dz'.$$

The z' integration limits are determined by the points where the integrand vanishes (see [45, 46]).

The current of magnetized electrons can be expressed as

$$j_e = q_e n_e c \frac{[\mathbf{E}\times\mathbf{B}]}{B^2} + \frac{c}{B^2}[\mathbf{B}\times\nabla_\perp p_{e\perp}] + c(p_{e\parallel} - p_{e\perp})\frac{[\mathbf{B}\times(\mathbf{B}\nabla)\mathbf{B}]}{B^4},$$

where q_e and n_e are the electron charge and number density, $p_{e\parallel}$ and $p_{e\perp}$ are the parallel and perpendicular components of the electron pressure, and $B = \sqrt{B_z^2 + B_x^2}$. Because the large-scale electric field E_y in the sheet can be eliminated by passing to a moving reference frame (the so-called de Hoffmann–Teller frame), only one nonvanishing electric field component $E_z = -d\varphi/dz$ is taken into account. The quasineutrality equation is used to find the scalar potential, $q_i n_i + q_e n_e = 0$. Hence, the TCS model is reduced to the Grad–Shafranov equation

$$\frac{dB_x}{dz} = \frac{4\pi}{c}\left[j_e(B_x, z) + j_i(B_x, z)\right],$$

where B_z can be considered a free parameter. The model obtained has a triple embedded structure. The electron current density profile with a sharp peak at the center is embedded into a wider profile of the ion current density. This structure as a whole is in turn embedded into a plasma sheet (the plasma density does not vanish at the CS boundary) (Fig. 2). The central peak of the electron current density is caused by the curvature drift, $\sim (p_{e\parallel} - p_{e\perp})/R_{curv}$, where the curvature radius R_{curv} is proportional to the ratio $(B_z/B_0)^2 \ll 1$.

Comparison of the model predictions with current sheets observed in the magnetotail showed that the model with transit particles allows describing the experimental data with a much better accuracy than the Harris model. Figure 3 shows an example of comparison of the current density profiles

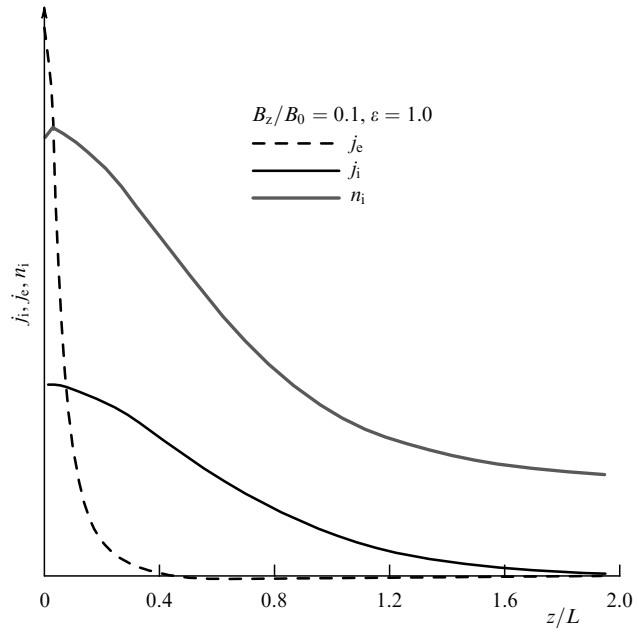

Figure 2. The profiles of the ion and electron current densities and plasma density for the TCS model.

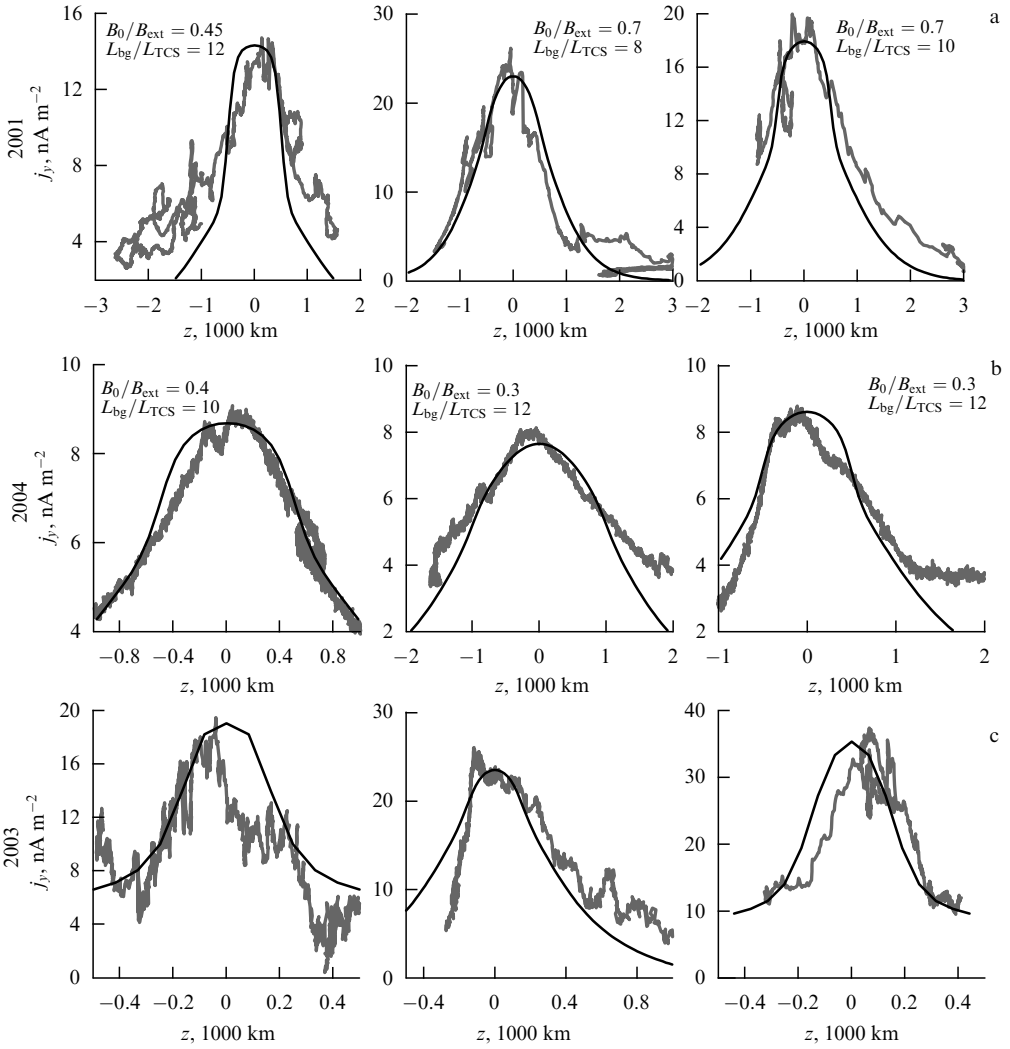

Figure 3. Profiles of the current density for the TCS model (black curves) and experimental observation (gray curves).

deduced from the direct measurement of the magnetic fields aboard the Cluster spacecraft with those calculated from the TCS model. We first consider Figs 3a and b. The data show that both the observed and modeled TCSs have an embedded structure with $B_0 < B_{ext}$. This characteristic feature of TCSs manifests itself in two different effects. The first is that for the events shown, the current density decreases by more than an order of magnitude, to $\sim 1-3$ nA m^{-2}, over distances of 1000–2000 km. As a result, the remaining magnetic field $B_{ext} - B_0$ is supported by a relatively weak background current; hence, the thickness of the background sheet L_{bg} is much larger than that of the TCS, L_{TCS}. Figures 3a and b also show the values for the ratio L_{bg}/L_{TCS} for the given current density profiles. The existence of a local strong current in a CS (emergence of a TCS) is therefore related to the emergence of a narrow strong CS within a wide CS, rather than to the narrowing of the entire CS.

The second effect is the emergence of a thin electron current within the ion TCS. Such structures can be resolved in spacecraft observations if the distance between the spacecraft is very small (≈ 300 km) (the Cluster spacecraft were working in this regime in 2003 [39]). The measured current density profiles are compared with the model results in Fig. 3c. It is seen from these plots that the model electron current is in good agreement with the measurements for profiles wider than 200 km. Hence, the double embedded structure of CSs predicted by the model in [46] is confirmed by the experimental data. Obviously, stability criteria for such structures should be entirely different from those for the Harris model.

It is worth noting that observations of very thin current sheets, where the electron current is much stronger than the ion current, are in good agreement with the results of Frank's group on laboratory modeling [1, Vol. 1, Ch. 9], [2, p. 108] that had been initiated by Syrovatskii.

The TCS model can be compared with experimental results in more detail by considering the distribution function of ions responsible for the currents. In the TCS model, the current is transferred by transit particles with a distinctive half-ring distribution function (see [47, 48]). An example of such a distribution function is shown in Fig. 4. The corresponding measurements are complicated by the presence of the background plasma. But because the background density (and the distribution function) does not change across a TCS (over scales ~ 1000 km), it is possible to subtract the distribution function measured at the current sheet boundary from that in the center of the TCS. A positive result then indicates the distribution of protons in the TCS (Fig. 5). Comparison of the model and the observed distributions shows that they are in good qualitative agreement (see Figs 4 and 5).

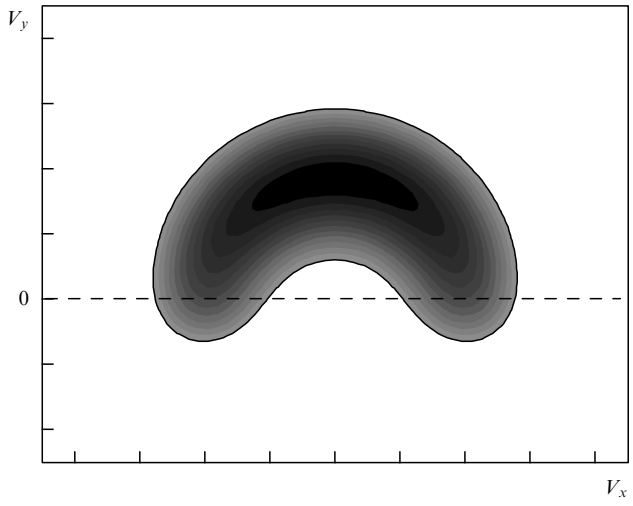

Figure 4. The distribution of the TCS transit particles.

Thus, a possible solution of the stability problem for the current sheet in the magnetotail may be found in using TCS models that are in better agreement with observations than the Harris model is.

3. Tearing instability

A comprehensive study of the tearing instability involves the variational method. To derive an equation for a perturbation of the vector potential $A_{1y} \sim \exp(\mathrm{i}kx - \mathrm{i}\omega t)$, the energy functional W_2 is calculated in the second order of the perturbation theory [49]. The functional W_2 contains three terms: the magnetic field perturbation energy W_B, the energy of the attraction of current filaments W_{free}, and a stabilizing contribution W_{e} due to the presence of the magnetic field B_z. The term W_{free} represents the 'free energy' of the system because this term allows the tearing instability to develop. The term W_{e} contains the contributions of several effects. First, the electrons are magnetized by B_z and, as the instability develops, their density is perturbed, $n_{1\text{e}} \sim B_{1z}/B_z$. Second, in order to maintain the plasma quasineutrality, the ions follow the electrons and this motion consumes a significant portion of the system free energy [26]. Third, the conservation of the canonical momentum $P_y = mv_y + qA_y/c \sim qB_z x/c$ implies additional restrictions on the tearing instability.

For the TCS model in [46], the three terms of the energy functional W_2 are as follows [51]:

$$W_B = \int \frac{(\nabla A_{1y})^2}{8\pi}\, \mathrm{d}^3 r\,,$$

$$W_{\text{free}} = -\frac{1}{2c}\int \frac{\partial j_0}{\partial A_{0y}}\, A_{1y}^2\, \mathrm{d}^3 r\,,$$

$$W_{\text{e}} = \int\left(\frac{q_{\text{i}} n_{0\text{i}}^2}{\partial n_{0\text{i}}/\partial\varphi_0}\,\frac{k^2}{B_z^2}\right) A_{1y}^2\, \mathrm{d}^3 r + W_H\,.$$

Here, the subscripts 0 denote the CS macroparameters in the unperturbed state (j_0 is the current, $n_{0\text{i}}$ is the ion density, A_{0y} is the only component of the vector potential, and φ_0 is the scalar potential). The term W_H is due to the dependence of P_y on B_z in the initial state and the corresponding additional restrictions for perturbations (see [49, 50]). The only component of the perturbed vector potential is A_{1y}. Actually, W_2 is the difference in the energies of the perturbed system and of the system in the initial state. Therefore, if there exists a function A_{1y} such that $W_2 < 0$, then the tearing instability development is energetically favorable and the CS is macroscopically unstable.

To verify this condition, it is necessary to solve the equation $\delta W_2/\delta A_{1y} = 0$, which determines A_{1y} for the minimum possible value of W_2. The solution of this equation is presented in [50]; here, we consider only the final result, i.e., the instability parameter domain shown in Fig. 6a. It is seen that thin and elongated current sheets with small ε and $B_z/B_0 \sim 0.1-0.2$ are unstable. Hence, the TCSs with an embedded structure not only resemble those in the experimental data but also allow solving the problem of the disruption of the magnetic field lines and substorm initialization due to a large amount of 'free' energy. In addition, predictions of the stability theory can be compared with experimental data.

We first see whether the observed TCSs have the properties that make the TCS model unstable. One of the main reasons for the TCS instability is a large amount of 'free energy,' which in turn manifests itself in the embedded structure of the sheet. A large difference between the spatial scales for the plasma density profile and those for the current density allows $\partial j_0/\partial A_{0y}$ to reach a large value, such that the energy variation W_2 becomes negative.

The effect considered can be estimated as follows. We first construct a simple empirical CS model that has an embedded structure and can be conveniently compared with experi-

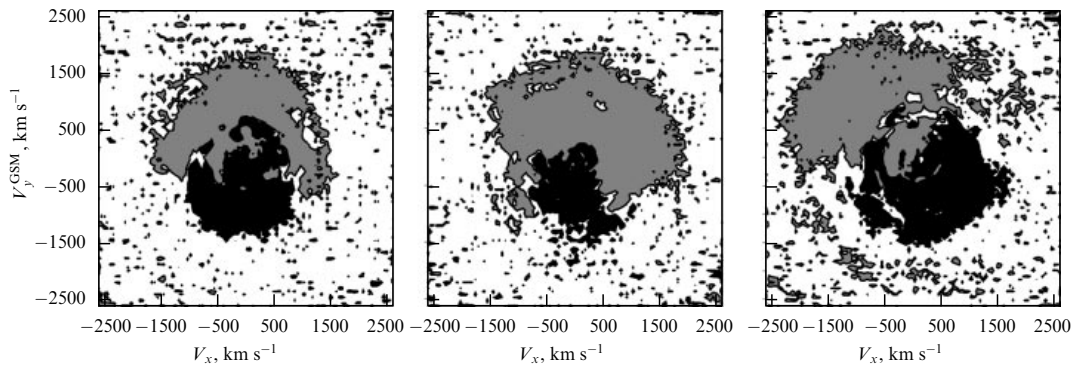

Figure 5. The proton distribution function in the central part of three TCSs. Gray color shows the population of particles that are present in the central part and responsible for the main current. (The superscript GSM stands for geocentric solar magnetospheric coordinates.)

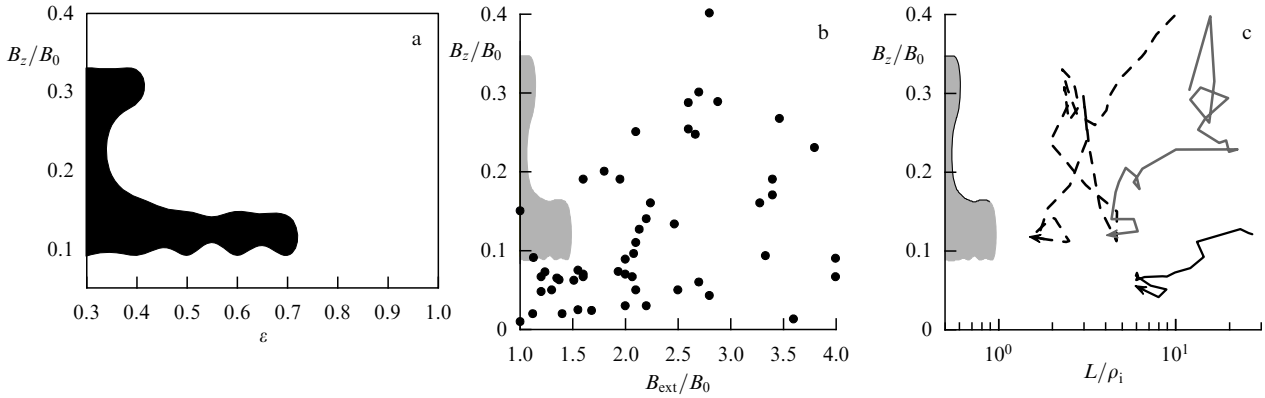

Figure 6. (a) A parametric map. Black color shows the region where $W_2 < 0$. (b) Map of the instability regions with the positions of the observed TCS. (c) A parametric instability map with the trajectories corresponding to CS evolution during the substorm growth phase.

mental data, and then estimate its free energy. We fix the amplitude of the external magnetic field $B_{\rm ext}$ (the value of the magnetic field where the plasma pressure vanishes), and the current density amplitude $j_{\max}$. Then the term corresponding to the TCS 'free energy' is given by

$$W_{\rm free} = -\frac{1}{2c}\int_{-\infty}^{+\infty}\frac{\partial j_0}{\partial A_{0y}}\,A_{1y}^2\,{\rm d}z = -\frac{j_{\max}}{cB_{\rm ext}}\int_0^1\frac{\partial j}{\partial b}\,\frac{1}{b}\,A_{1y}^2\,{\rm d}b\,,$$

where $b = B_x/B_{\rm ext}$ and $j = j_0/j_{\max}$. We next consider the structure of the current sheets on the (b, j) plane. In the Harris model, the current density is $j = \cosh^{-2}(z)$ and the magnetic field is $b = \tanh(z)$. Hence, the model is represented by the parabola $j = 1 - b^2$. The simple model of an embedded TCS has the only free parameter, the value of the magnetic field at the TCS boundary, $b_0 < 1$. The current density in this model is the sum of two currents if we consider that in the region $b > b_0$, there is only the background current $j_{\rm bg} = j_1(1 - b^2)$ and in the region $b < b_0$, the TCS current $j_{\rm TCS} = j_0(1 - b^2/b_0^2)$ is added to that current. In this case, a relation between the model parameters can be established: at the TCS center ($z = 0$, $b = 0$), the total current is equal to 1, $j_1 + j_0 = 1$, and at the boundary ($b = b_0$), it is equal to a number μ. With j_1 and j_0 expressed in terms of the model parameters, it is possible to find an equation for the total current both in the central region and outside the sheet:

$$j = 1 - \left(\frac{b}{b_0}\right)^2(1-\mu)\,,\quad b < b_0\,,$$

$$j = \frac{\mu(1-b^2)}{1-b_0^2}\,,\quad b > b_0\,.$$

Hence, the 'free energy' is given by

$$W_{\rm free} \sim -\frac{2j_{\max}}{cB_{\rm ext}}\left(\frac{1-\mu}{b_0^2} + \frac{\mu}{1-b_0^2}\right).$$

On the other hand, in the Harris model, $\partial j/\partial b = -2b$ and

$$W_{\rm free} = -\frac{2j_{\max}}{cB_{\rm ext}}\int_0^1 A_{1y}^2\,{\rm d}b \sim -\frac{2j_{\max}}{cB_{\rm ext}}\,.$$

Therefore, the ratio of the estimated free energies of a TCS and a Harris CS is determined by the coefficient $s = (1-\mu)b_0^{-2} + \mu(1-b_0^2)^{-1}$. As $\mu \to 0$ and $b_0 \to 1$, the TCS transforms into the Harris CS and $s \to 1$. This coefficient can be found for all observed TCSs. We have chosen eight TCS events observed by Cluster and calculated s using the empirical model (Fig. 7). It follows from the plots that the free energy estimates obtained with such a crude technique are larger by a factor of 2–3 for some observed TCSs than the estimates for the Harris CS.

Another possibility of comparing theoretical results with experimental data is provided by the obtained parametric map with instability regions (Fig. 6a). The positions of observed CSs can be shown on this map. For this, it is necessary to transform the parameter ε into an observed parameter. The pressure balance at the TCS boundary allows obtaining a relation between the amplitude of the TCS magnetic field B_0 and the plasma pressure $P_{\rm b}$ at the TCS boundary (see [45]). Using this relation and the definition of the field $B_{\rm ext}$ ($P_{\rm b} + B_0^2/8\pi = B_{\rm ext}^2/8\pi$), we obtain

$$\frac{B_{\rm ext}^2}{B_0^2} = 1 + \varepsilon^2\left\{1 + \frac{\varepsilon\exp(-\varepsilon^{-2})}{\sqrt{\pi}\left[1+\operatorname{erf}(\varepsilon^{-1})\right]}\right\}^{-1}.$$

We note that the electron contribution to the pressure balance is neglected here (this contribution is small because the ion temperature should be larger than that for electrons by a factor of 5–7). Hence, the parameter ε can be transformed into measurable parameters.

We now use statistical data [51] for observed TCSs and show their positions on the instability parameter map. We can argue that a TCS observed under quiet conditions should fall outside the instability region. It can be seen from Fig. 6b that this statement is true. Only two observed events fall into the instability region. Most observed events occupy a zone around the instability region in the parameter space, thereby confirming the metastability concept, i.e., the current sheets 'live' in the magnetotail for several tens of minutes; however, the observations show that they are close to the instability region. This means that a quasistationary state of the system can change spontaneously (in $\sim 1-2$ min) to a rapid development of the tearing instability.

The obtained instability map can be compared with the observed evolution of the CS at the substorm growing phase. In this case, it is more convenient to use a theoretical relation between the parameter ε and the TCS thickness measured in the ion gyroradii $L/\rho_{\rm i}$ (see [45]). For this, we can use experimental observations [52] of the CS evolution before a substorm. A summary is presented in Fig. 6c: during this

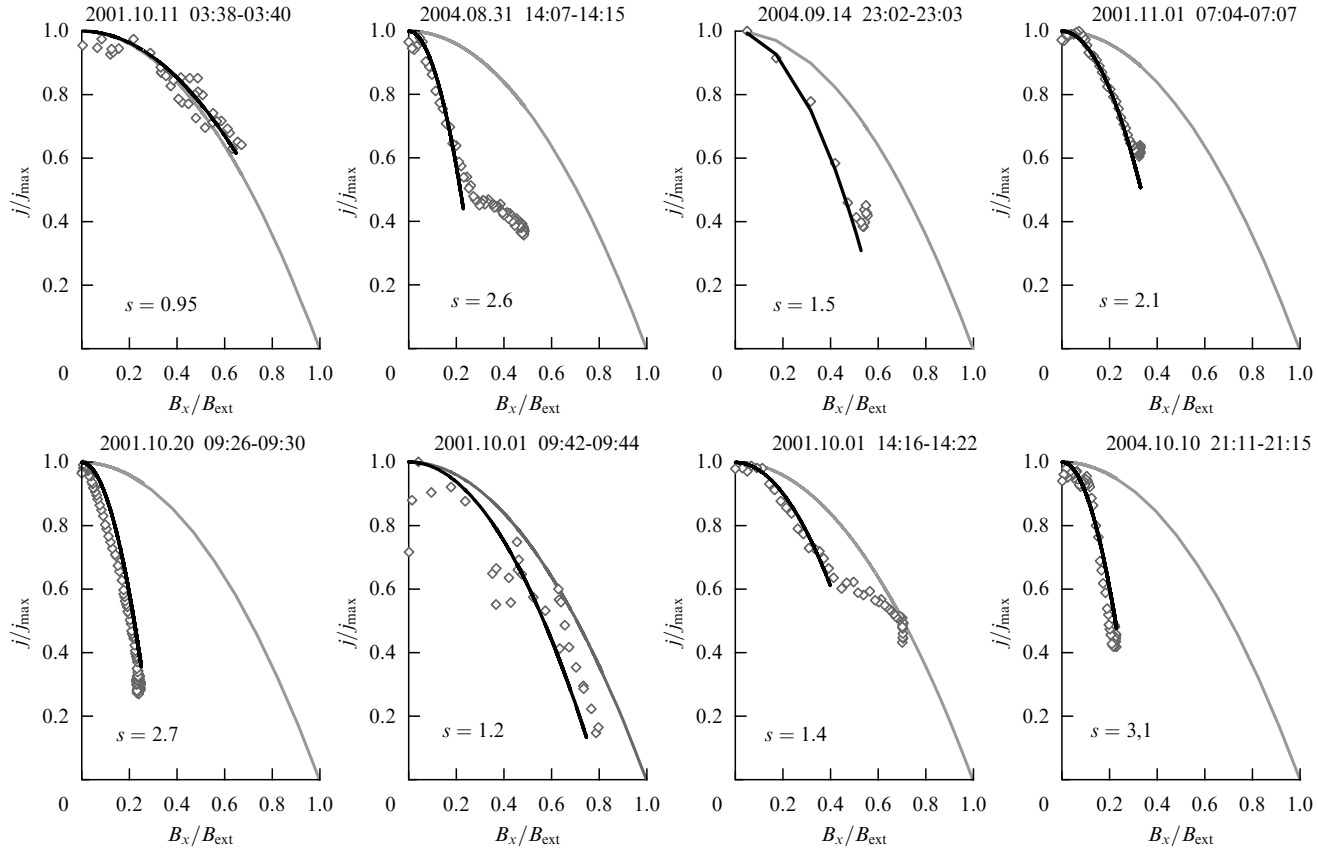

Figure 7. The profiles for the observed TCSs (open rhombi), approximation of the profiles by the function $j = 1 - \alpha b^2, \alpha = \text{const}$ (black curve) and profile for the Harris model (gray curve). Also shown are the corresponding values of s.

evolution, both the thickness and the ratio B_z/B_0 decrease, with the CS approaching the instability region. All the experimental observations used here show that at the next stage of the CS evolution, the disruption of magnetic field lines is unavoidable.

In summary, the TCS stability theory, which accounts for the mechanisms of their metastability, is strongly supported by experimental data.

4. Discussion: dynamics of a current sheet

A stability analysis of TCSs showed that in addition to the tearing instability, various drift modes with $k_y \neq 0$ can also develop [53]. This may lead to the pinching of magnetic surfaces, as well as to their bending. In this process, the growth rates for drift modes are larger than those for the tearing mode. This is closely related to the fact that the drift modes only deform magnetic surfaces without breaking them. As a result, the electron density perturbations and, consequently, the stabilizing contribution of the electrons to the energy functional W_2 becomes negligible. Under realistic conditions with a three-dimensional CS, the drift modes develop first, and then the tearing instability can develop in the background of the deformed magnetic surfaces. Hence, instead of infinite one-dimensional X-lines, which emerge during the current filamentation in the sheet and the corresponding field line reconnection, the system contains magnetic islands, which are bounded not only in the x direction but also in the y direction. This fact is not so important for substorm initialization. But it is more important for the nonlinear phase of various instabilities in the tail and particle acceleration, which are influenced by such a complicated topological structure of the magnetic surfaces.

Because the influence of the magnetic field on the particle motion in the vicinity of an X-line is small, the particles can be accelerated by an inductive electric field emerging in dynamical processes in the CS. If the electric field is regarded as a uniform external field acting on particles in the region of an X-line, then the plasma particles can be considerably accelerated (up to hundreds of keV in the magnetotail [54] and several MeV in the solar corona [55]) and non-Maxwellian particle distributions can be formed. The applications of such models to the solar [19, 21] and magnetospheric [56, 57] plasmas are widely discussed. On the other hand, it is possible to consider a nonstationary field line reconnection directly. In this case, the electric field is induced and the particle acceleration occurs in pulses [23, 58]. A comparison of spacecraft observations in the magnetotail with theoretical predictions confirms the validity of this approach to the interpretation of short-lived bursts of accelerated charged particles [59].

However, the spatial localization of X-lines does not allow accelerating large numbers of charged particles. This restriction may be obviated if there exists a magnetic field $B_y \neq 0$. In this case, the magnetic field disruption may result in a number of X-lines [60]. The particle acceleration in such structures was previously studied in the context of magnetopause CSs [61].

The drift-mode instabilities developing in a TCS with a subsequent deformation of the magnetic surfaces may result in a similar complex web-like structure of X-lines in the

current sheet in the magnetotail. In this case, the development and interaction of different unstable modes result in a turbulent electromagnetic field [62]. The particle acceleration by these fields is efficient enough in the approximation of strongly disrupted magnetic surfaces, when the particles stay near the CS neutral plane for a long time [63], as well as when the turbulence only deforms the magnetic field lines, allowing particles to escape from the CS after a short time [64]. In both cases, the populations of accelerated particles may form high-energy 'tails' of non-Maxwellian distributions, which are often observed in Earth's magnetosphere and solar corona.

When a multimode instability develops, the formation of large-scale magnetic structures (plasmoids) may result from the interaction of individual small magnetic islands formed by the disruption of CS magnetic surfaces. Using the kinetic [65] and magnetohydrodynamic [66] approaches, it was shown that a nonlinear stage exists such that the attraction of currents carried by a number of magnetic islands make the islands merge and form a large-scale structure.

5. Conclusions

We have reviewed modern models and experimental data related to thin current sheets and studied the effect of the coexistence of different scales in its structure on the tearing instability. It was shown that experimental observations of the evolution of current sheets in the magnetotail and, on the other hand, theoretical models for TCSs lead to the metastability concept suggested by Syrovatskii [2, 12] and Galeev [26]. Theoretical results show that a region exists in the parameter space where the tearing instability can develop. Outside this region, stable current sheets may exist for very long periods of time and accumulate the solar wind energy, even if the sheets are strongly squeezed and stretched. Then, when they enter the instability region, the energy is released and transformed into the kinetic energy of fluxes of accelerated particles. The experimental data confirm that most TCSs observed in the magnetotail are metastable, and their positions on the parameter map determine the limits of the time periods when they are stable with respect to the tearing instability. In addition, experimental data on the evolution of current sheets in the substorm growing phase indicate that the sheets approach the instability region as they move on the parameter map.

Summarizing the results of this paper, we note that the metastability concept, which explains the alternation of long-lasting preparatory phases and rapid releases of accumulated energy, is now used in the modern theory of magnetospheric substorms [1].

The research was supported by the RFBR grants 10-05-91001 and 10-02-93114-NTsNIL and the grant NSh-320.2010.2.

References

1. Zelenyi L M, Veselovskii I S (Eds) *Plazmennaya Geliogeofizika* (Plasma Helio-geophysics) (Moscow: Fizmatlit, 2008)
2. Basov N G (Ed.) *Neitral'nye Tokovye Sloi v Plazme* (Neutral Current Sheets in Plasmas) (Proc. (Trudy) of the P N Lebedev Phys. Inst., Vol. 74) (Moscow: Nauka, 1974) [Translated into English (New York: Consultants Bureau, 1976)]
3. Priest E R *Rep. Prog. Phys.* **48** 955 (1985)
4. Vainshtein S I, Bykov A M, Toptygin I N *Turbulentnost', Tokovye Sloi i Udarnye Volny v Kosmicheskoi Plazme* (Turbulence, Current Sheets, and Shock in Cosmic Plasma) (Moscow: Nauka, 1989) [Translated into English (Langhorne, Pa.: Gordon and Breach Sci. Publ., 1993)]
5. Istomin Ya N *Astron. Zh.* **82** 500 (2005) [*Astron. Rep.* **49** 446 (2005)]
6. Panov E V et al. *J. Geophys. Res.* **113** A01220 (2008)
7. Giovanelli R G *Mon. Not. R. Astron. Soc.* **107** 338 (1947)
8. Sweet P A, in *Electromagnetic Phenomena in Cosmical Physics* (Proc. IAU Symp., No. 6, Eds B Lehnert) (Cambridge: Cambridge Univ. Press, 1958) p. 123
9. Vasyliunas V M *Rev. Geophys. Space Phys.* **13** 303 (1975)
10. Biskamp D *Nonlinear Magnetohydrodynamics* (Cambridge: Cambridge Univ. Press, 1993)
11. Semenov V S, Drobysh O A, Heyn M F *Adv. Space Res.* **19** 1793 (1997)
12. Syrovatskii S I *Zh. Eksp. Teor. Fiz.* **60** 1727 (1971) [*Sov. Phys. JETP* **33** 933 (1971)]
13. Basov N G (Ed.) *Vspyshechnye Protsessy v Plazme* (Flare Processes in Plasmas) (Trudy FIAN , Vol. 110) (Moscow: Nauka, 1979)
14. Ness N F *J. Geophys. Res.* **70** 2989 (1965)
15. Harris E G *Nuovo Cimento* **23** 115 (1962)
16. Schindler K *Astrophys. Space Sci. Library* **32** 200 (1972)
17. Lembege B, Pellat R *Phys. Fluids* **25** 1995 (1982)
18. Coppi B, Laval G, Pellat R *Phys. Rev. Lett.* **16** 1207 (1966)
19. Bulanov S V, Sasorov P V *Astron. Zh.* **52** 763 (1975) [*Sov. Astron.* **19** 464 (1975)]
20. Somov B V, Syrovatskii S I *Usp. Fiz. Nauk* **120** 217 (1976) [*Sov. Phys. Usp.* **19** 813 (1976)]
21. Bulanov S V *Pis'ma Astron. Zh.* **6** 372 (1980) [*Sov. Astron. Lett.* **6** 206 (1980)]
22. Galeev A A, Coroniti F V, Ashour-Abdalla M *Geophys. Res. Lett.* **5** 707 (1978)
23. Galeev A A *Space Sci. Rev.* **23** 411 (1979)
24. Galeev A A, Zelenyi L M *Pis'ma Zh. Eksp. Teor. Fiz.* **22** 360 (1975) [*JETP Lett.* **22** 170 (1975)]
25. Schindler K *J. Geophys. Res.* **79** 2803 (1974)
26. Galeev A A, Zelenyi L M *Zh. Eksp. Teor. Fiz.* **70** 2133 (1976) [*Sov. Phys. JETP* **43** 1113 (1976)]
27. Coroniti F V *J. Geophys. Res.* **85** 6719 (1980)
28. Galeev A A, Sudan R N (Eds) *Osnovy Fiziki Plazmy* (Basic Plasma Physics) (Moscow: Energoatomizdat, 1983, 1984); *Basic Plasma Physics* (Amsterdam: North-Holland, 1983, 1984)
29. Buechner J, Zelenyi L M *J. Geophys. Res.* **92** 13456 (1987)
30. Pellat R, Coroniti F V, Pritchett P L *Geophys. Res. Lett.* **18** 143 (1991)
31. Quest K B, Karimabadi H, Brittnacher M *J. Geophys. Res.* **101** (A1) 179 (1996)
32. Lui A T Y *J. Geophys. Res.* **101** (A6) 13067 (1996)
33. Petrukovich A A et al. *J. Geophys. Res.* **103** (A1) 47 (1998)
34. Baumjohann W et al. *Adv. Space Res.* **25** 1663 (2000)
35. Petrukovich A A et al. *J. Geophys. Res.* **114** A09203 (2009)
36. Angelopoulos V et al. *Science* **321** 931 (2008)
37. Sergeev V A et al. *J. Geophys. Res.* **98** (A10) 17345 (1993)
38. Asano Y et al. *Geophys. Res. Lett.* **32** L03108 (2005)
39. Nakamura R et al. *Space Sci. Rev.* **122** 29 (2006)
40. Runov A et al. *Ann. Geophys.* **24** 247 (2006)
41. Artemyev A V et al. *Ann. Geophys.* **26** 2749 (2008)
42. Speiser T W *J. Geophys. Res.* **70** 4219 (1965)
43. Büchner J, Zelenyi L M *J. Geophys. Res.* **94** (A9) 11821 (1989)
44. Kropotkin A P, Domrin V I *J. Geophys. Res.* **101** (A9) 19893 (1996)
45. Zelenyi L M et al. *Nonlin. Proces. Geophys.* **7** 127 (2000)
46. Zelenyi L M et al. *Nonlin. Proces. Geophys.* **11** 579 (2004)
47. Ashour-Abdalla M, Büchner J, Zelenyi L M *J. Geophys. Res.* **96** (A2) 1601 (1991)
48. Burkhart G R et al. *J. Geophys. Res.* **97** (A9) 13799 (1992)
49. Schindler K *Physics of Space Plasma Activity* (Cambridge: Cambridge Univ. Press, 2007)
50. Zelenyi L et al. *J. Atm. Solar-Ter. Phys.* **70** 325 (2008)
51. Zelenyi L M, Artemyev A V, Petrukovich A A *Geophys. Res. Lett.* **37** L06105 (2010)
52. Petrukovich A A et al. *J. Geophys. Res.* **112** A10213 (2007)
53. Zelenyi L M et al. *Ann. Geophys.* **27** 861 (2009)
54. Christon S P et al. *J. Geophys. Res.* **94** 13409 (1989)

55. Shcherbina-Samoilova I S (Ed.) *Itogi Nauki i Tekhniki. Astronomiya* (Progress in Science and Technology. Astronomy) Vol. 32 (Moscow: VINITI, 1987)
56. Hoshino M *J. Geophys. Res.* **110** A10215 (2005)
57. Pritchett P L *J. Geophys. Res.* **111** A10212 (2006)
58. Zelenyi L M, Lominadze J G, Taktakishvili A L *J. Geophys. Res.* **95** 3883 (1990)
59. Taktakishvili A L et al. *Kosmich. Issled.* **36** 282 (1998) [*Cosmic Res.* **36** 265 (1998)]
60. Galeev A A, Kuznetsova M M, Zelenyi L M *Space Sci. Rev.* **44** 1 (1986)
61. Drake J F et al. *Nature* **443** 553 (2006)
62. Zelenyi L M, Milovanov A V *Usp. Fiz. Nauk* **174** 809 (2004) [*Phys. Usp.* **47** 749 (2004)]
63. Zelenyi L M et al. *Phys. Lett. A* **372** 6284 (2008)
64. Artemyev A V et al. *Nonlin. Proces. Geophys.* **16** 631 (2009)
65. Zeleny L M, Taktakishvili A L *Plasma Phys. Control. Fusion* **30** 663 (1988)
66. Pella R *Fiz. Plazmy* **9** 204 (1983)

PACS numbers: 52.30.Cv, 52.35.Vd, 96.60.Q–
DOI: 10.3367/UFNe.0180.201009h.0982

Dynamics of current sheets underlying flare-type events in magnetized plasmas

A G Frank

1. Introduction

Sergei Ivanovich Syrovatskii was a remarkable physicist who made an outstanding contribution to magnetohydrodynamics, the physics of cosmic rays, astrophysics, and solar physics. His classic review on magnetohydrodynamics [1] published in *Physics–Uspekhi* in 1957 is well known. At the end of the 1950s and in the 1960s, Syrovatskii, in close collaboration with V L Ginzburg, actively worked on astrophysical problems related to cosmic rays. *The Origin of Cosmic Rays* by Ginzburg and Syrovatskii [2] was published in 1963, republished several times in this country and abroad, and is still widely cited.

In the early 1960s, Syrovatskii focused on processes on the Sun, especially those involving considerable numbers of particles accelerated during solar flares. By that time, it had been discerned from observational data that the source of tremendous energies released during solar flares is the energy of the magnetic fields generated by electric currents in the solar corona. In 1966, Syrovatskii wrote a pioneering paper on this subject, "Dynamic dissipation of a magnetic field and particle acceleration" [3], where he considered a general nonstationary problem of compressible plasma flows in a two-dimensional inhomogeneous magnetic field with a neutral line. He reached the fundamental conclusion that the flows of a highly conductive plasma in such a field results in a considerable energy accumulation and the emergence of a current sheet separating the oppositely directed magnetic fields [3, 4]. The magnetic energy concentrated in the vicinity of the current sheet can be released in the case of rapid sheet disruption resulting in the emergence of strong electric fields, which accelerate charged particles. In accordance with Syrovatskii's concept, the cumulation of magnetic energy and the formation of current sheets precedes the flares. A flare occurs when the sheet is disrupted and the magnetic reconnection releases the accumulated energy, which is transformed into the thermal and kinetic energy of the plasma, fluxes of energetic particles, and radiation in different parts of the electromagnetic spectrum.

Syrovatskii suggested the idea that a cumulative acceleration occurs during the flares, when all particles in a small region are accelerated, regardless of their properties; the acceleration is therefore spatially nonuniform. The cumulative acceleration differs considerably from statistical acceleration, when a small population of particles that differ from other particles by some parameters, for instance, by the initial energy, mass, or charge, is accelerated. In addition, Syrovatskii emphasized that "a process of the rapid dissipation of the magnetic field, which is accompanied by the emergence of energetic particles" is quite ubiquitous and may occur not only in solar flares but also in many other dynamic phenomena in space and laboratory plasmas [3].

The first experiments on plasma dynamics in two-dimensional (2D) magnetic fields with neutral lines were performed in the early 1970s in the USA, Japan, and the USSR, in the Laboratory of Accelerators at the Lebedev Physical Institute. Although these studies were independent of each other, they were quite similar in many aspects and, as it turned out later, all the experiments were inspired by Syrovatkii's papers published in 1966–1971.

One of the investigation directions in the Laboratory of Accelerators, Lebedev Physical Institute in that period was related to the development of physical principles for new plasma methods for acceleration of charged particles. That is why Syrovatskii's ideas were of special interest. Syrovatskii and the head of the laboratory M S Rabinovich pioneered the decision to make a relatively small experimental setup and to investigate the possibility of cumulative acceleration. It is difficult to describe the enthusiasm with which Syrovatskii participated in the discussions of the basic principles, parameters, and construction of this setup. We note that experimental decisions suggested at the initial stage of the studies stood the test of time and were used in all subsequent setups from the 'current sheet' (CS) family.

2. Is it possible to accumulate the magnetic energy in the laboratory?

Experiments performed at the Lebedev Physical Institute were focused on studies in a parameter range as wide as possible. With this aim, three independent electrotechnical systems were used in the CS setup [5]. These were, first, a system responsible for the 2D magnetic field with a neutral line on the z axis, field lines in the (x, y) plane, and a radial gradient h of the field:

$$\mathbf{B} = \{B_x; B_y; B_z\} = \{-hy; -hx; 0\}\,; \qquad (1)$$

second, a system that created an initial plasma in the magnetic field; and third, a system creating an electric current J_z parallel to the neutral line (Fig. 1a).

It was expected that two-dimensional plasma flows emerging with currents would result in the accumulation of the magnetic energy in the vicinity of the neutral line, and that

A G Frank Prokhorov General Physics Institute,
Russian Academy of Sciences, Moscow, Russian Federation
E-mail: annfrank@fpl.gpi.ru

Uspekhi Fizicheskikh Nauk **180** (9) 982–988 (2010)
DOI: 10.3367/UFNr.0180.201009h.0982
Translated by V V Lobzin; edited by A M Semikhatov

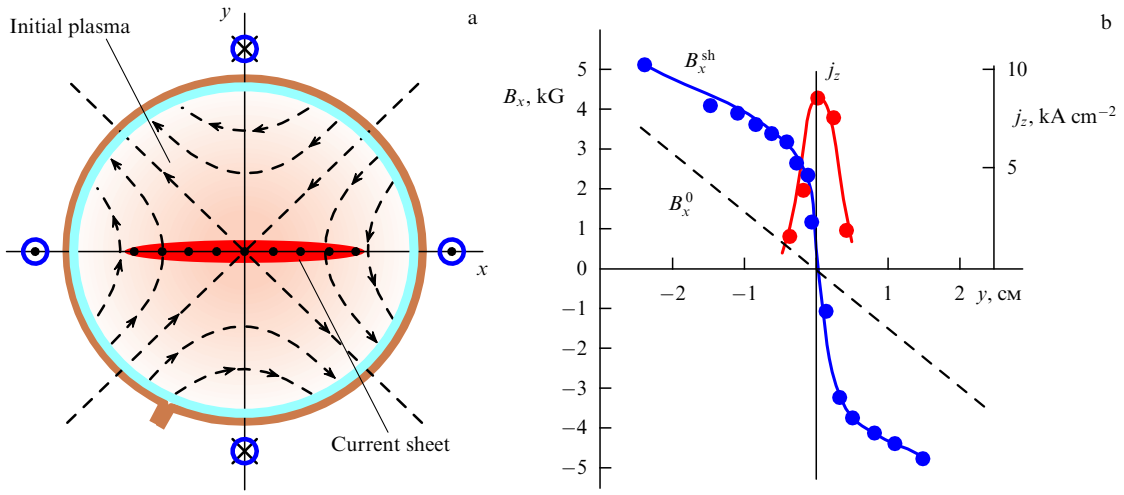

Figure 1. (a) A cross section of the 'current sheet' setup (Lebedev Physical Institute). A 2D magnetic field with the field lines (dashed lines) in the (x, y) plane and a neutral line on the z axis is created by the four straight conductors, which are parallel to the vacuum chamber axis. The initial plasma in the magnetic field is created by theta discharge in the neutral gas. The current excitation directed along the z axis results in current sheet formation. (b) The magnetic field increase and concentration of the magnetic energy in the vicinity of the neutral line as a result of the current sheet formation. B_x^{sh} is the magnetic field component tangential to the sheet surface; B_x^0 is the same component before the development of the current sheet; j_z is the current density in the sheet. Shown are the dependences of these parameters in the direction of the normal to the sheet, i.e., along the y axis.

a current sheet would develop. But the first experiments performed at the Lebedev Physical Institute gave negative results, i.e., the accumulation was not achieved. Currents in the plasma resulted in a sharp conductivity decrease due to plasma instabilities, such that the freezing-in condition for the plasma magnetic field did not hold.

To check the freezing-in condition, a dimensionless parameter, the magnetic Reynolds number $\mathrm{Re_m}$ is typically used. If

$$\mathrm{Re_m} = \frac{4\pi\sigma L v}{c^2} \gg 1\,, \tag{2}$$

then the magnetic field moves with the plasma, i.e., it is frozen in the substance. Here, σ is the plasma conductivity, and L and v are a characteristic scale of the plasma and its characteristic velocity. Condition (2) is certainly valid for almost all astrophysical objects, first of all due to their giant sizes L, while in laboratory experiments, it is necessary to create a plasma with a high conductivity σ to satisfy condition (2). To solve this problem, a crucial idea was suggested that the plasma conductivity can be increased by a considerable increase in the initial electron density. This allowed increasing the conductivity to $\sigma \approx 2 \times 10^{14}$ s^{-1}, such that the freezing-in condition held for several microseconds [6].

As a consequence, a neutral current sheet separating the regions with oppositely directed magnetic fields was obtained for the first time and a significant (several dozenfold) increase in the magnetic energy density was achieved in the vicinity of the CS surface (Fig. 1b) [6]. The process of CS formation in the 2D magnetic field with a neutral line has been studied, from the linear stage with a propagating magnetosonic wave to the nonlinear stage of energy accumulation. The detailed structure of the magnetic field created by currents in the plasma was determined and it was shown that the currents are shaped as sheets [7]. These results provided an additional argument for resolving the dilemma of Syrovatskii's CS [8] or a Petchek-type flow [9], and favored the CS [10].

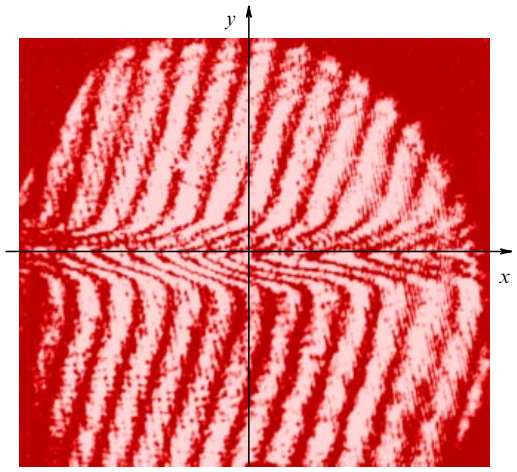

Figure 2. The interferogram characterizing the 2D electron density distribution in the current sheet. The double-exposure holographic interferometry technique was used.

An important stage of the experimental studies was the 'visualization' of the plasma compressed to a flat sheet, i.e., obtaining a vivid 2D plasma density distribution by means of holographic interferometry (Fig. 2) [11]. It was found that as a current sheet develops, a rapid and effective compression of the plasma occurs, resulting in a 10–15-fold density increase with respect to both the initial plasma density and the density outside the sheet. The electron and ion temperatures are also much higher in the sheet than outside. In other words, a current sheet is a spatial region where a dense and hot plasma is concentrated, with the plasma pressure being balanced by the magnetic pressure outside the layer and a characteristic plasma parameter $\beta \approx 1$. Here,

$$\beta = \frac{8\pi N_e (T_e + T_i/Z_i)}{(B_x^{sh})^2}\,, \tag{3}$$

N_e, T_e, T_i, and Z_i are respectively the electron density, electron and ion temperatures, and the mean ion charge in the middle plane of the sheet, and B_x^{sh} is the tangential component of the magnetic field near the sheet surface.

An unexpected but very important result was that the sheet is quite stable [11, 12]: it can exist without any changes in the magnetic field structure and distributions of plasma density over extended periods, which are much longer than the characteristic times for the tearing instability [13]. This result, which shows that the magnetic energy can be gradually increased in the vicinity of current sheets over prolonged periods, is extremely important for astrophysical applications [14].

Thus, in the experiments that were carried out in 1970–1980s and dedicated to studies of the plasma dynamics in 2D magnetic fields with neutral lines, the processes typical for pre-flare conditions were realized, namely, a considerable accumulation of the magnetic energy resulting from the emergence of metastable current sheets, the plasma heating in the sheets, and the generation of plasma fluxes.

3. Transition to three-dimensional magnetic configurations

In Nature, just as in plasma laboratory setups (for instance, in tokamaks), the magnetic configurations are usually three-dimensional (3D), i.e., have all three components of the magnetic field. In addition, 3D configurations are not only more common in the real world but are also more general in comparison with the 2D configurations with a neutral line and enhanced symmetry. In this connection, an obvious question arises of whether it is possible to accumulate the magnetic energy in 3D configurations.

The problem of a 3D generalization of the results obtained for 2D magnetic fields with neutral lines was widely discussed in the literature. Using the magnetohydrodynamic (MHD) equations describing the plasma dynamics in the vicinity of X-type neutral lines, Syrovatskii proved the possibility of current sheets forming in 3D configurations that combine 2D magnetic fields with neutral lines and a relatively uniform longitudinal field B_z:

$$\mathbf{B} = \{B_x; B_y; B_z\} = \{-hy; -hx; B_z\}\,, \tag{4}$$

$$\frac{\partial B_z}{\partial z} \ll h\,. \tag{5}$$

Under condition (5), the longitudinal component can play a role analogous to that of thermal pressure. These ideas by Syrovatskii were confirmed by subsequent experiments.

At the same time, several theoretical studies [16–19] considered the plasma flows in spatially nonuniform 3D magnetic fields with isolated neutral points. From self-similar solutions of the MHD equations, it was possible to conclude that the existence of a region with a vanishing magnetic field is necessary for the formation of a current sheet in a 3D magnetic configuration.

Experimental studies of plasma dynamics and energy transformations in 3D configurations were commenced in the 1990s in different laboratories worldwide, including the Plasma Physics Department of the Prokhorov Institute for General Physics, Russian Academy of Sciences, with a new-generation CS-3D facility (Fig. 3). One of the main goals of the experiments was to find the 3D magnetic field characteristics that are required for energy accumulation in plasmas.

Three-dimensional magnetic configurations with topological peculiarities such as neutral points or neutral lines are

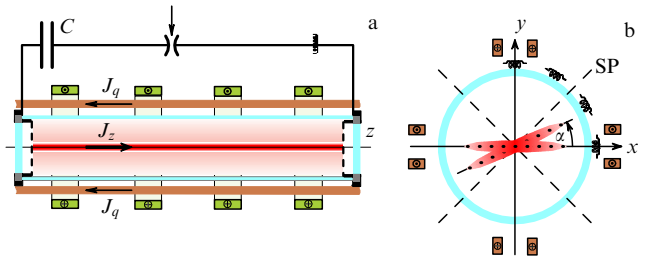

Figure 3. The design of the 3D CS experimental facility. (a) The side view. (b) A cross section [22]. The dashed lines in panel (b) show the orientation of the separatrix planes (SP) for the 2D magnetic field with a neutral line.

created in the 3D CS setup by superposing two magnetic fields with different (translational and axial) symmetries [20]. A magnetic field with the translational symmetry is the 2D field given by (1), with a neutral line on the z axis. As axially symmetric magnetic fields with the z axis directed along the neutral line, three types of fields were used: uniform magnetic fields B_z satisfying condition (5), 3D nonuniform magnetic fields with one or several neutral points, and 3D nonuniform fields without neutral points. The intensities of each of the two fields, as well as the structure of the axially symmetric field, can be changed independently of one another, thereby providing both a variety of initial configurations and a gradual transition between different configurations.

In a 3D magnetic configuration, a plasma is created and then an electric current J_z is generated along the neutral line of the 2D magnetic field, the line coinciding with the symmetry axis of the axially symmetric field. The energy used in the 3D CS facility to create the magnetic fields is $W \approx 400$ kJ, the initial plasma density varies in the range $\approx 10^{16}-10^{14}$ cm^{-3}, magnetic fields can reach ≈ 10 kG, and the plasma current is $J_z \approx 100$ kA.

4. Current sheets in 3D magnetic configurations with neutral points

The first experiments on the 3D CS setup were performed for 3D magnetic fields with isolated neutral points, when the axially symmetric field was that of the 'anti-mirror machine,'

$$\mathbf{B}^{A} = \{h_A x;\, h_A y;\, -2h_A z\}\,. \tag{6}$$

Here, the neutral line of the anti-mirror machine is at the origin, and h_A is the radial gradient of the magnetic field in the vicinity of the neutral point.

If the 2D magnetic field with the neutral line on the z axis is given by

$$\mathbf{B}^{q} = \{hx;\, -hy;\, 0\}\,, \tag{7}$$

where h is the radial gradient, then it is easy to see that a superposition of fields (6) and (7) forms a new 3D magnetic field $\mathbf{B}^{\Sigma}$ with a neutral point. In the vicinity of the neutral point, the structure of the magnetic field depends on the ratio of the gradients h_A and h [20]:

$$\begin{aligned}\mathbf{B}^{\Sigma} &= \mathbf{B}^{q} + \mathbf{B}^{A} = \{(h+h_A)x; (-h+h_A)y;\, -2h_A z\} \\ &= h\{(1+\gamma)x; (-1+\gamma)y;\, -2\gamma z\}\,,\end{aligned} \tag{8}$$

$$\gamma = \frac{h_A}{h}\,. \tag{9}$$

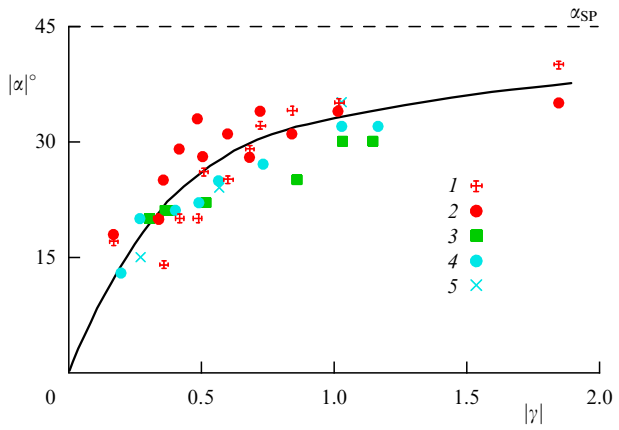

Figure 4. The dependence of the angular orientation $|\alpha|$ of the current sheet in the (x, y) plane on the parameter $|\gamma|$ for nonuniform 3D magnetic fields. Results *1* and *5* were obtained from the images of the radiating plasma, and *2–4* from the magnetic measurements. Data points *1* and *2* correspond to the sheet position in the vicinity of the magnetic neutral point, and data points *3–5* were obtained far away from the neutral point and in the magnetic field without neutral points [21].

It was found that a current sheet does form in the vicinity of the neutral point of the 3D magnetic field, and the plane of the sheet is rotated by an angle α with respect to the position of the sheet in the 2D field [21]. The angle α increases with increasing h_A and decreasing h, i.e., it depends on the parameter γ in (9) and varies in the range $0 \leqslant |\alpha| \leqslant \pi/4$ as $|\gamma|$ increases (Fig. 4, data points *1* and *2*) [21]. Therefore, the formation of current sheets in 3D magnetic fields with neutral points does occur; moreover, it occurs in a large variety of such configurations.

It was found that the current sheet is formed not only in the vicinity of the neutral point but also far from it, in regions with a sufficiently strong longitudinal magnetic field B_z, as well as in nonuniform magnetic fields without neutral points. In each cross section $z = \text{const}$, the angular orientation of the sheet is determined by the local value of the parameter $\gamma(z) = h_A(z)/h$ (see Fig. 4, data points *3–5*) [21]. The variation of the angular position of the sheet depending on the value of $\gamma(z)$ results the current sheet taking the form of a bended surface in a nonuniform magnetic field [22].

From the experimental data obtained, it was found that a critical condition for a sheet to develop in a 3D magnetic field is the presence of singular X-type lines with a saddle-like transverse structure [22]. We note that the 3D magnetic field with a neutral point also has an X-line. Without loss of generality, this allowed studying the evolution of current sheets in 3D fields (4) with a uniform longitudinal component $B_z \approx \text{const}$ directed along the X-line [23]. Such a field can be regarded as an element of a more complex 3D magnetic configuration with spatially varying components.

5. Current sheets in 3D magnetic configurations with X-lines

In passing from 2D configuration (1) to 3D configuration (4), a question arises as to how much the longitudinal component B_z affects the possibility of a current sheet developing and the current sheet parameters. Experiments performed with 3D magnetic fields (4) with different combinations of longitudinal and transverse components allowed establishing that a necessary condition for a current sheet to develop is that the gradient of the transverse field exceed a critical value, $h > h^{cr}$ [23]. In this case, the magnetic field B_z may exceed the transverse field in the entire region occupied by the plasma [24].

Detailed studies of the structure of current sheets developing in 3D configurations (4) showed that the distributions of currents are shaped like sheets, and the magnetic structures of the sheets in the 2D and 3D configurations are very similar [25]. As in the case of 2D fields, the plasma can be compressed by a factor of 5–10 compared with its initial density in 3D magnetic fields with the longitudinal component B_z [26].

In addition, the studies revealed that the compression ratio for the magnetic field and the current forming the sheet decreases as the magnetic field B_z increases [25, 26]. This effect manifests itself, first, in decreased values of the maximum current and plasma densities and, second, in an increased thickness of the sheet, i.e., in its smaller transverse size [25, 26]. The decreased compression ratio results in a sharp decrease in the plasma density gradient perpendicular to the sheet surface, whereas the total number of electrons per unit (1 cm) of thickness does not change considerably (Fig. 5a) [26]. In other words, as the B_z component increases in configuration (4), the plasma dynamics tend to those of incompressible plasmas.

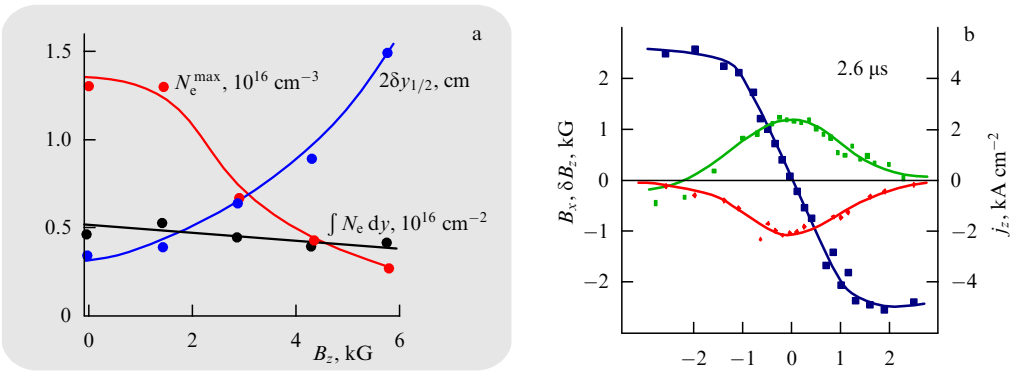

Figure 5. (a) The dependences of the maximum electron density N_e^{max} in the sheet, the sheet thickness $2\delta y_{1/2}$ (level $0.5N_e^{max}$), and the number of electrons per cm of the sheet thickness on the longitudinal magnetic field B_z [26]. (b) Transverse (along the y axis) distributions of the tangential component of the magnetic field B_x, the current density j_z, and the longitudinal magnetic field δB_z trapped in the sheet.

These results allowed suggesting that the decreased compression of the plasma on the sheet is caused by the increased B_z magnetic field component compared with its value outside the sheet [26]. Indeed, a gradual increase in the longitudinal component was observed in magnetic measurements [27]. The excess of the longitudinal magnetic field in the sheet compared with its initial value reached $\delta B_z \geqslant 1.2$ kG (Fig. 5b) and, importantly, the direction of the field δB_z captured in the sheet always coincided with the direction of the B_z component in the initial configuration (4).

The increased longitudinal magnetic field in the current sheet can exist only due to plasma currents in the (x, y) plane. In this case, the total current responsible for the δB_z field attained $J_x \approx 57$ kA, i.e., its order of magnitude was close to that of the main current, $J_z \approx 70$ kA. As a consequence, the current structure becomes three-dimensional as the current sheet develops in a 3D magnetic field.

A current sheet that forms in 3D magnetic field (4) appears as a region with concentrated hot and dense plasma, like sheets in 2D fields. The electron temperature and plasma density, the ion temperature, and the effective ion charge attain maximum values in the middle plane of the sheet and increase with time [28]. But the increase in the longitudinal magnetic field in the sheet by δB_z changes the condition of the transverse equilibrium of the sheet,

$$N_e\left(T_e + \frac{T_i}{Z_i}\right) + \frac{(\delta B_z)^2}{8\pi} \approx \frac{(B_x^{sh})^2}{8\pi}\,, \qquad (10)$$

$$\beta < 1\,.$$

It follows from this equation that the magnetic pressure of the transverse field B_x^{sh}, which compresses the plasma and current onto the sheet, is balanced by the sum of the thermal plasma pressure $N_e(T_e + T_i/Z_i)$ and the magnetic pressure due to the field δB_z [28]. It is worth emphasizing that the analogy between the pressure of the longitudinal magnetic field and the plasma pressure was substantiated by Syrovatskii in [15].

Hence, in 3D nonuniform magnetic fields with X-lines of different structures, extended current sheets may develop, with a considerable amount of magnetic energy concentrated in their vicinity. The sheets may exist for a long time without changes in their structure and parameters, i.e., they are metastable.

6. Two-fluid effects in current-sheet plasmas

In studies of current sheets developing in 3D magnetic configurations with an X-line and a longitudinal magnetic field B_z, the emergence of deformed (i.e., bended and asymmetric) current sheets was observed [29]. The asymmetry became more prominent as the ion mass was increased in the plasmas under study. This phenomenon was interpreted as a manifestation of two-fluid effects in the current-sheet plasma, namely, the generation of Hall currents in the sheet. In the presence of the B_z component, these currents give rise to additional dynamic effects causing sheet deformation [29]. As the direction of the B_z component was changed, the current sheet orientation changed as well, thereby confirming this hypothesis.

The analysis of the plasma parameters showed that the sheet deformation and consequently the generation of Hall currents occurred under the condition that the velocity u_c of the electrons carrying the current is several times larger than

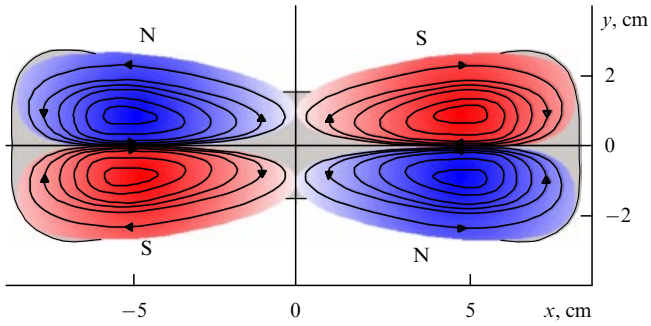

Figure 6. The structure of the Hall currents in the cross section of a current sheet. In the (x, y) plane, the Hall currents form four closed contours, which create a quadrupole longitudinal magnetic field B_z in the sheet [30]. In two quadrants placed diagonally, the B_z component is directed to the observer (N), while in the others it is directed from the observer (S).

the characteristic Alfvén speed v_A,

$$u_c \gg v_A\,. \qquad (11)$$

Obviously, condition (11) can hold not only in 3D configurations (4) with B_z components but also in 2D fields with neutral lines (1), when $B_z = 0$ and the plasma sheets are planar and symmetric. It would appear reasonable that in the symmetric current sheets, Hall currents could be generated by the electrons moving with respect to heavy and slow-moving ions. In this case, the sheet remains symmetric because in the absence of the B_z component, there are no forces deforming the sheet.

Direct measurements revealed the generation of a longitudinal magnetic field B_z in the current sheets developing in 2D magnetic configurations. It is worth emphasizing that the B_z component was absent in both the initial 2D field and the magnetic field created by the main current J_z in the sheet [30]. Emerging in the current sheet, the longitudinal B_z component has a characteristic quadrupole structure and its appearance is direct evidence of the generation of Hall currents in the sheets.

The structure of Hall currents was determined for the first time and it was shown that in the current sheet cross section, i.e., in the (x, y) plane, the Hall currents form four current contours that create a quadrupole longitudinal magnetic field B_z (Fig. 6) [30]. The magnitude of the total Hall current along the current sheet reaches $J_H \approx 130-150$ kA. The Hall currents exist in the sheet for a limited time, which increases with the ion mass. The acceleration of ions along the surface of the current sheet, from the center to the lateral borders, results in the damping of the Hall currents. Thus, the generation of Hall currents in a sheet created in a 2D magnetic field considerably complicates the current and magnetic field structures, making them three-dimensional.

Currently, manifestations of two-fluid effects in the magnetic reconnection in current sheets, including the process in Earth's magnetosphere, are attracting particular attention.

7. Disruption of the current sheet and flare phenomena

The long-lasting phase in which a current sheet is stable and accumulates a considerable amount of magnetic energy created serious complications for laboratory experiments aimed at disrupting the sheet, releasing the accumulated

energy, and thereby realizing a flare event. Regarding this problem, Syrovatskii suggested that the relatively tenuous external plasma surrounding the current sheet prevents the disruption of the sheet by repairing the emerging disruptions [31]. Using this concept and experimental data on the dynamics of the peripheral plasma [32], it has been possible to find current sheet formation conditions such that a pulsed phase of magnetic reconnection occurs spontaneously and results in a catastrophic disruption of the current sheet [12]. The typical features of the pulsed phase are an abrupt change in the magnetic field topology, redistribution of currents in the sheet, the appearance of super-Alfvénic waves, and the generation of plasma flows [33, 34].

Rapid rearrangement of the magnetic field in the sheet result in excitation of the inductive electric fields and acceleration of the plasma particles. Indeed, the generation of accelerated electrons with energies exceeding 10 keV always correlated in time with the pulsed phase of the magnetic reconnection, i.e., with the current sheet disruption [35]. The most energetic particles were observed at the initial phase of the sheet disruption, thereby demonstrating a qualitative analogy with the particle acceleration during solar flares.

Thus, at the pulsed phase of the magnetic reconnection in current sheets in laboratory plasmas, all main nonstationary processes typical for flare events were observed; these include a rapid sheet disruption and release of accumulated magnetic energy, strong plasma heating and ejection from the sheets, and acceleration of charged particles [36, 37]. Recent preliminary results have demonstrated a possibility of rapid disruption of the current sheets created in 3D magnetic configurations.

The question of the physical mechanisms responsible for the long-lasting metastable phase of the current sheet evolution, initiation of the rapid disruption of the sheet, and flare phenomena is still open. On the one hand, at the pulsed phase of the magnetic reconnection, a decrease in the plasma conductivity [38] and increase in anomalous electric fields [39] are observed, thereby giving evidence of turbulent processes in the sheet plasma. But there are reasons to suppose that the plasma turbulence does not initiate the reconnection; rather, the turbulence is a consequence of reconnection.

It was found that an unusually rapid increase in the electron and ion temperatures occurs in a relatively small region within the current sheet just before the pulsed phase of the magnetic reconnection [40–42]. From the experimental data collection, a conclusion can be made that the pulsed plasma heating in the 'hot spots' of the current sheet is probably the main reason for violation of the transverse equilibrium of the sheet, its disruption, and, finally, release of the accumulated magnetic energy [42]. It is worth emphasizing that the crucial role of thermal processes causing the current sheet disruption is similar to the role of the 'thermal trigger' for solar flares considered by Syrovatskii [43].

8. Conclusions

The results of experimental studies allow arguing that flare phenomena in plasmas may have their origin in the evolution and dynamics of current sheets, as was predicted by Syrovatskii. Accumulation of the magnetic energy in plasmas occurs in the vicinity of metastable current sheets as they are forming in both 2D and 3D magnetic fields with neutral X-lines. A rapid disruption of the current sheet results in the release of the accumulated magnetic energy, which transforms into the thermal plasma energy and the energy of suprathermal fluxes of the plasma and of accelerated particles. The most probable cause of the termination of the metastable stage and the beginning of the pulsed phase of the magnetic reconnection seems to be thermal processes related to the pulsed local plasma heating.

Currently, a number of laboratories in different countries are deeply involved in experimental studies targeted at the investigation of the current sheets and magnetic reconnection in plasmas (for details, see [44] and the references therein). These studies commenced in the 1970s under the influence of the ideas of Syrovatskii.

References

1. Syrovatskii S I *Usp. Fiz. Nauk* **62** 247 (1957)
2. Ginzburg V L, Syrovatskii S I *Proiskhozhdenie Kosmicheskikh Luchei* (The Origin of Cosmic Rays) (Moscow: Izd. AN SSSR, 1963) [Translated into English (Oxford: Pergamon Press, 1964)]
3. Syrovatskii S I *Astron. Zh.* **43** 340 (1966) [*Sov. Astron.* **10** 270 (1966)]
4. Syrovatskii S I *Zh. Eksp. Teor. Fiz.* **50** 1133 (1966) [*Sov. Phys. JETP* **23** 755 (1966)]
5. Syrovatskii S I, Frank A G, Khodzhaev A Z *Zh. Tekh. Fiz.* **43** 912 (1973) [*Sov. Phys. Tech. Phys.* **18** 580 (1973)]
6. Syrovatskii S I, Frank A G, Khodzhaev A Z *Pis'ma Zh. Eksp. Teor. Fiz.* **15** 138 (1972) [*JETP Lett.* **15** 94 (1972)]
7. Frank A G, in *Neitral'nye Tokovye Sloi v Plazme* (Neutral Current Sheets in Plasmas) (Proc. (Trudy) of the P N Lebedev Phys. Inst., Vol. 74, Ed. N G Basov) (Moscow: Nauka, 1974) p. 108 [Translated into English (New York: Consultant Bureau, 1976) p. 107]
8. Syrovatskii S I *Zh. Eksp. Teor. Fiz.* **60** 1727 (1971) [*Sov. Phys. JETP* **33** 933 (1971)]
9. Petchek H E, in *The Physics Solar Flares, Proc. of the AAS–NASA Symp., 28–30 October, 1963, Greenbelt, MD* (Ed. W N Hees) (Washington, DC: NASA, 1964) p. 425
10. Syrovatskii S I, in *Neitral'nye Tokovye Sloi v Plazme* (Neutral Current Sheets in Plasmas) (Proc. (Trudy) of the P N Lebedev Phys. Inst., Vol. 74, Ed. N G Basov) (Moscow: Nauka, 1974) p. 3 [Translated into English (New York: Consultant Bureau, 1976) p. 3]
11. Dreiden G V et al. *Fiz. Plazmy* **3** 45 (1977) [*Sov. J. Plasma Phys.* **3** 26 (1977)]
12. Kirii N P et al. *Fiz. Plazmy* **3** 538 (1977) [*Sov. J. Plasma Phys.* **3** 303 (1977)]
13. Furth H P, Killeen J, Rosenbluth M N *Phys. Fluids* **6** 459 (1963)
14. Syrovatskii S I *Izv. Akad. Nauk SSSR Ser. Fiz.* **43** 695 (1979)
15. Syrovatskii S I *Annu. Rev. Astron. Astrophys.* **19** 163 (1981)
16. Rosenau P *Phys. Fluids* **22** 849 (1979)
17. Bulanov S V, Olshanetskii M A *Fiz. Plazmy* **11** 727 (1985) [*Sov. J. Plasma Phys.* **11** 425 (1985)]
18. Lau Y-T, Finn J M *Astrophys. J.* **350** 672 (1990)
19. Greene J M *Phys. Fluids B* **5** 2355 (1993)
20. Bulanov S V, Frank A G *Fiz. Plazmy* **18** 1535 (1992) [*Sov. J. Plasma Phys.* **18** 795 (1992)]
21. Bogdanov S Yu et al. *Pis'ma Zh. Eksp. Teor. Fiz.* **59** 510 (1994) [*JETP Lett.* **59** 537 (1994)]
22. Frank A G *Plasma Phys. Control. Fusion* **41** (3A) A687 (1999)
23. Bogdanov S Yu et al. *Pis'ma Zh. Eksp. Teor. Fiz.* **71** 78 (2000) [*JETP Lett.* **71** 53 (2000)]
24. Frank A G, Bogdanov S Yu *Earth Planets Space* **53** 531 (2001)
25. Bogdanov S Yu et al. *Fiz. Plazmy* **33** 483 (2007) [*Plasma Phys. Rep.* **33** 435 (2007)]
26. Frank A G et al. *Phys. Plasmas* **12** 052316 (2005)
27. Frank A, Bugrov S, Markov V *Phys. Lett. A* **373** 1460 (2009)
28. Voronov G S et al. *Fiz. Plazmy* **34** 1080 (2008) [*Plasma Phys. Rep.* **34** 999 (2008)]
29. Frank A G et al. *Phys. Lett. A* **348** 318 (2006)
30. Frank A G, Bugrov S G, Markov V S *Phys. Plasmas* **15** 092102 (2008)
31. Syrovatskii S I *Izv. Akad. Nauk SSSR Ser. Fiz.* **39** 359 (1975) [*Bull. Acad. Sci. USSR Phys. Ser.* **39** (2) 96 (1975)]

32. Bogdanov S Yu et al. *Fiz. Plazmy* **1** 133 (1975) [*Sov. J. Plasma Phys.* **1** 71 (1975)]
33. Bogdanov S Yu, Markov V S, Frank A G *Pis'ma Zh. Eksp. Teor. Fiz.* **35** 232 (1982) [*JETP Lett.* **35** 290 (1982)]
34. Bogdanov S Yu et al. *Phys. Scripta* **30** 282 (1984)
35. Bogdanov S Yu, Markov V S, Frank A G *Pis'ma Zh. Eksp. Teor. Fiz.* **51** 563 (1990) [*JETP Lett.* **51** 638 (1990)]
36. Syrovatskii S I *Vestn. Akad. Nauk SSSR* (10) 33 (1977)
37. Syrovatskii S I *Priroda* (2) 143 (1978)
38. Frank A G, in *Voprosy Fiziki Plazmy i Plazmennoi Elektroniki* (Plasma Physics and Plasma Electronics) (Proc. (Trudy) of the P N Lebedev Phys. Inst., Vol. 160, Ed. L M Kovrizhnykh) (Moscow: Nauka, 1985) p. 93 [Translated into English (Commack, N.Y.: Nova Science Publ., 1989) p. 131]
39. Frank A G et al. *Contrib. Plasma Phys.* **36** 667 (1996)
40. Kirii N P, Markov V S, Frank A G *Pis'ma Zh. Eksp. Teor. Fiz.* **48** 419 (1988) [*JETP Lett.* **48** 459 (1988)]
41. Beigman I L et al. *Zh. Prikl. Spektrosk.* **54** 1021 (1991)
42. Kirii N P, Markov V S, Frank A G *Pis'ma Zh. Eksp. Teor. Fiz.* **56** 82 (1992) [*JETP Lett.* **56** 82 (1992)]
43. Syrovatskii S I *Pis'ma Astron. Zh.* **2** 35 (1976) [*Sov. Astron. Lett.* **2** 13 (1976)]
44. Yamada M, Kurlsrud R, Ji H *Rev. Mod. Phys.* **82** 603 (2010)

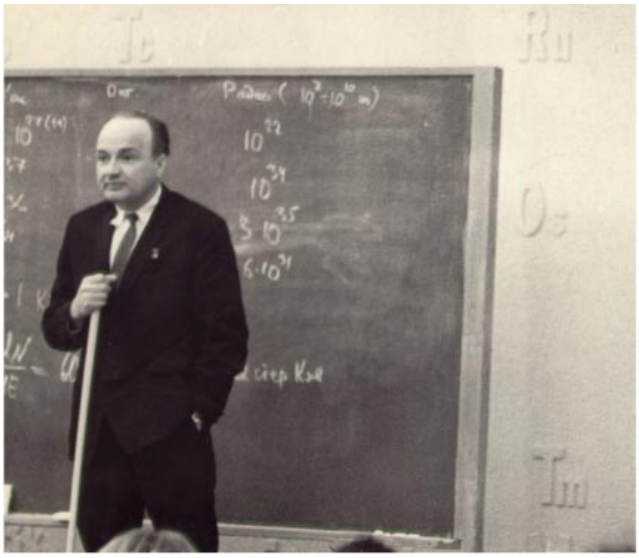

Sergei Ivanovich Syrovatskii. A seminar talk.

PACS numbers: **07.87.+v**, 52.35.Vd, **96.60.–j**
DOI: 10.3367/UFNe.0180.201009i.0988

Space research of the Sun

V D Kuznetsov

1. Introduction

When speaking about solar studies, we first mean the Sun, our nearest star, as an astrophysical object that interests us because of both purely scientific (astrophysical) and practical aspects (since the Sun influences Earth and our life). Solar physics embraces various physical areas: nuclear physics, plasma physics and magnetic hydrodynamics (MHD), radiophysics, atomic physics and spectroscopy, and so on. All these physical directions are currently part of modern astrophysics as well.

The Sun is a natural space laboratory accessible for detailed investigation. Solar observations provide vast valuable data for understanding the Sun's composition and workings, and testing current theories and models applied for describing plasma, MHD, and other processes in space conditions, in particular, in distant astrophysical objects (e.g., convection, dynamo, and active phenomena). Currently, we can speak of heliophysics science, because solar and heliospheric physics are inseparably linked with each other [1]. It is appropriate that to mark the 50th anniversary of the International Geophysical Year, 2007 was named the International Heliophysical Year. Recently, the most significant progress in solar studies has been due to spacecraft studies; spacecraft allow observing the Sun in electromagnetic spectral ranges inaccessible from Earth, in the X-ray and ultraviolet ranges (extraterrestrial astronomy), as well as carrying out local measurements of plasma fluxes and particles emitted directly from the Sun. Elimination of the atmospheric influence for observations from space have provided a higher quality of optical observations, even though the size of space telescopes is always limited in comparison with ground-based terrestrial ones.

In the 1970s, Sergei Ivanovich Syrovatskii's main scientific interests were related to solar studies, magnetic reconnection and solar flares, and space, mostly solar, MHD — the fields where he is one of the classics. He paid considerable attention to observations of the Sun and its active atmospheric phenomena, whose origin and physics were quite interesting and not fully understood. Observations were regularly discussed at his seminar, and the theory of current sheets and magnetic reconnection was originated [1, 2], which was the basis for developed models of solar flares [3, 4] and other active phenomena. Observations with a high spatial resolution were not available at that time; this, on the one hand, provided a base for different approaches to explanations of phenomena and for discussions, and, on the other hand, set out the task of developing high-resolution space observations, which were eventually realized and have confirmed Syrovatskii's ideas.

2. Solar space projects

The current period in solar studies is called the golden era of solar physics in space, because such numbers of spacecraft and related results have never been seen before in the history of space research. Table 1 presents solar space projects of previous years, separated into four parts: recently completed, current, in preparation, and under development. A separate column shows the worthy contributions of Russian projects to this area of research.

In Sections 3–7, a brief review is given of the main results of solar space studies, from the solar interior to the solar wind. In Section 8, future solar space projects are described. A more detailed account can be found in Refs [5–7].

According to the current model, the Sun has a core where energy releasing thermonuclear fusion reactions occur; a radiation zone, throughout which the radiation energy released in the core is transferred to outer regions; the convective zone, the most outward invisible shell where the

V D Kuznetsov Pushkov Institute of Terrestrial Magnetism, Ionosphere, and Radio Wave Propagation, Russian Academy of Sciences, Troitsk, Moscow region, Russian Federation. E-mail: kvd@izmiran.ru

Uspekhi Fizicheskikh Nauk **180** (9) 988 – 996 (2010)
DOI: 10.3367/UFNr.0180.201009i.0988
Translated by S V Vladimirov; edited by A M Semikhatov

Table 1. Recent solar space projects *

	USA, Europe, Japan	Russia
Completed	Ulysses (1990 – 2009)	CORONAS-F (2001 – 2005) CORONAS-FOTON (2009)
Current	SOHO (1995) TRACE (1998) RHESSI (2002) Hinode (2006) STEREO (2006) SDO (2009)	
In preparation	Solar Probe + (2018)	Interhelioprobe (> 2014)
Under development	Solar orbiter (> 2017) Sentinels Polaris, etc.	Polar–Ecliptic Patrol (PEP)
* In brackets are spacecraft launching years and operation periods.		

Figure 1. Structure of the current inside the Sun and on its surface (SOHO result).

energy transfer to external regions occurs through convection; the atmosphere, including the visible solar outer shells: the photosphere, chromosphere, transition region, and corona transiting to solar wind. The presentation below follows this solar structure, from the core to the solar wind.

3. Solar interior and helioseismology

The Sun's interior is investigated from space by observing its global oscillations, whose amplitude, manifested in fluctuations of radiation fluxes, plasma density, and velocity, is small enough to require high-precision measurements (10^{-6}) achieved in extraterrestrial observations. There are two types of solar global oscillation modes transferring information about the solar interior: G-modes (with a period greater than 30 min), which are yet undetected, and p-modes (with a period of the order of 5 min), which are actively being investigated by helioseismology methods [8]. About 10–15 high-amplitude p-mode harmonics can be detected simultaneously [9, 10]; with time, some modes disappear and others appear. One of the interpretations invokes the convection effect, which has a wide noise spectrum, on natural harmonic oscillations inside the Sun. Frequency splitting of p-mode global oscillations due to the Sun's rotation has been recorded; this provides information on the angular velocity of the inner region rotations.

Figure 1 shows the solar rotation and inner layer current picture according to helioseismology data [MDI (Michelson Doppler Imager) instrument aboard the SOHO (Solar and Heliophysics Observatory) spacecraft]. The rotation is differential, with the angular velocity depending on the radius and latitude, which makes the pattern of motions quite complex. The darker color corresponds to velocities above the average, and the lighter color to velocities below the average. At the equator, the rotation speed is higher, decreasing in moving to the poles. On the Sun's surface, bright zones rotate slightly faster, and sun spots tend to appear at the boundaries of these regions. There is a slow meridional current flowing from the equator to the poles; it is closed at the bottom of the convective zone. This flow plays an important role in the solar dynamo and in the description of the solar cycle.

With the use of acoustic tomography methods (local helioseismology), it is possible to reconstruct the pressure (or speed of sound) distribution in subphotospheric layers and on the invisible solar side surface [11, 12]; this is important for localization of magnetic fluxes emerging from under the photosphere and that of active regions before they appear on the visible solar side and for increasing the longer-term forecast reliability for solar sporadic activity.

4. Solar atmosphere

The solar atmosphere, ranging from the photosphere to corona (photosphere, chromosphere, transition zone, and corona), is observed in various spectral lines, each of which corresponds to a particular plasma temperature and a solar atmosphere slice at a particular altitude. Multiwave observations thus provide a possibility to reconstruct the altitudinal (three-dimensional) picture of the solar atmosphere and various formations. This imaging spectroscopy method was successfully used in a number of solar projects: SOHO, CORONAS-F (Russian for complex orbital near-Earth observations of solar activity), STEREO (Solar–TErrestrial RElation Observatory), CORONAS-FOTON, Hinode, and SDO (Solar Dynamics Observatory).

At the photospheric level, observations with a high spatial resolution allowed detailed investigations of the convection and the granulation related to it, developed in the form of bright isolated surface regions corresponding to rising hot plasma. These regions are separated by dark 'corridors' forming a continuous network of sinking cooled plasma. A typical granular size is 0.2 arc seconds or 140 km. Between the cells, a background magnetic field about 400 G at the photospheric level is 'grabbed' by the counter-streaming plasma flows, and magnetic flux tubes are formed with a high field intensity up to a few kG. These tubes, predicted earlier [13, 14] and discovered by Hinode data [15], strongly affect the solar atmospheric dynamics, thus demonstrating the important role of the fine structure of the magnetic field.

The subphotospheric structure of plasma flows in a sunspot (the principal magnetized plasma formation of the solar photosphere) was investigated by acoustic tomography methods [11]. It was unclear for a long time how sunspots with high magnetic fields (2000–4000 G) can remain stable, instead of decaying within a few weeks and Sun revolutions (one

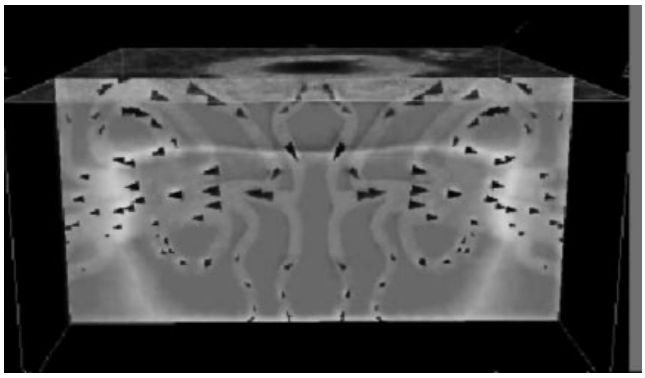

Figure 2. The subphotospheric flow structure around a sunspot providing its long-term stability (SOHO result).

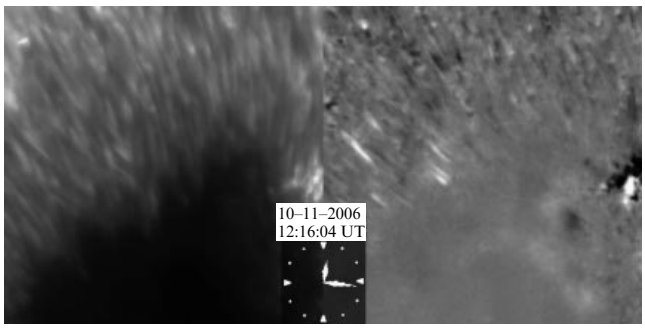

Figure 3. Multiple magnetic reconnection processes in a sunspot, accompanied by plasma ejections (Hinode result).

revolution every 27 days). The sunspots are surprisingly shallow in depth, changing from being colder than their environment to hotter than the environment at only 5000 km below the surface level. At the photospheric level, gas outflow from the sunspot occurs, and at the chromospheric and coronal level, there is gas inflow. Immediately below the surface, theoretically predicted plasma fluxes flowing inside the sunspot have been observed. At various depths under the photosphere, a system of two oppositely circulating toroidal vortices is formed around the sunspot magnetic tube, thus ensuring the long-term sunspot stability (Fig. 2).

According to high-temporal-resolution Hinode observations, numerous micro-ejections due to multiple magnetic reconnection processes of the 'uncombed' (entangled) magnetic field lines near a sunspot (Fig. 3) exist in the sunspot penumbra [16]. These ejections last for about 1 min, their speed is more than 50 km s^{-1}, and they are observed everywhere in the penumbra.

After the photosphere, in the next (by height) solar atmospheric layer, the chromosphere, high-spatial-resolution studies embraced the filamentary structure, spicules, prominences and the motion of substance there, other formations, and plasma heating effects in the vicinity of sunspots.

The structure and dynamics of the solar atmosphere, from the photosphere to the corona, are largely determined by magnetic fields. In the corona, magnetic forces substantially dominate over plasma pressure forces. High-spatial-resolution observations have allowed investigating the magnetic field structure, topology, and dynamics from the photosphere to the corona in detail. All of the Sun's surface is covered by a magnetic 'carpet' [17] with a complex, multiply connected field topology: the field emerging from one source (sunspot) is closed on several other sources. For such a topology, a set of null points and neutral (null) and limit field lines is formed, through which topologically disconnected magnetic fluxes are redistributed. In these regions, according to Syrovatskii's theory, current sheets are formed and the related magnetic reconnection occurs, leading to topological rearrangement of the magnetic field and to phenomena such as flares and mass ejections [3]. In the magnetic field structure, loop magnetic structures dominate at various scales, from the smallest to gigantic ones. Sometimes they form arcades, and the loops are often twisted and undergo eruption. The shapes of plasma structures and plasma dynamics that are determined by magnetic fields are amazing in their originality: surfacing magnetic fluxes, the growth and rise of coronal loops, local ejections and plasma motions along the field, sunspot rotation and related coronal effects, transverse oscillations of coronal loops, ejections of twisted magnetic tubes and prominences, and so on. The Sun's atmosphere clearly demonstrates phenomena and processes that find an explanation in MHD, providing us with a natural plasma laboratory.

In a quiet solar atmosphere, the density monotonically decreases with height, and the temperature starts to increase in the transition zone, increasing in the corona by 200 and more times [$(1-2) \times 10^6$ K] compared with the photospheric temperature (~ 6000 K). One of the solar physical and astrophysical problems is the coronal heating. In addition, there exists the related problem of solar wind acceleration, which we discuss in Section 6.

Despite long-term and intensive studies of the Sun's coronal heating problem, there is still no unique and final answer as regards the coronal heating mechanism. The questions of where the energy comes from, how it is transferred into the corona, and how it dissipates in the corona have not yet been answered. Several mechanisms are being considered. One of them is the heating by waves coming from below: they are generated by the convective zone, converted into Alfvén waves, and propagate upward, into the corona. For a long time, there were no observational confirmations of this mechanism. According to high-temporal-resolution Hinode coronal observations [18, 19], it was possible to detect wave oscillations coming from below, giving support to a more detailed analysis of the wave mechanism contribution to the coronal heating.

Another coronal heating mechanism is related to multiple microreconnection processes in magnetic tubes, where the field is characterized by flux ropes twisted owing to chaotic motions in the photosphere [20]. There are ubiquitous observations by Hinode spacecraft [21] of small local ejections in various directions that accompany the magnetic reconnection process.

On the Sun, an entire hierarchy of energy release processes occurs, from large flares with an energy of the order of 10^{32} erg to micro- and nanoflares, with energies 10^{-6} and 10^{-9} times less. The last are observed as bright X-ray sunspots located even in quiet solar regions and polar zones. They are actually very small loop structures existing almost everywhere. These observations significantly changed the 'quiet Sun' concept, which assumed an equilibrium in the absence of nonthermal processes characteristic for bright X-ray sunspots. From that standpoint, the Sun is never quiet, and coronal heating occurs continuously and at various scales. The Sun's largest-scale hot formations with temperatures 10–20 times higher than the corona temperature were observed by CORONAS-F space-

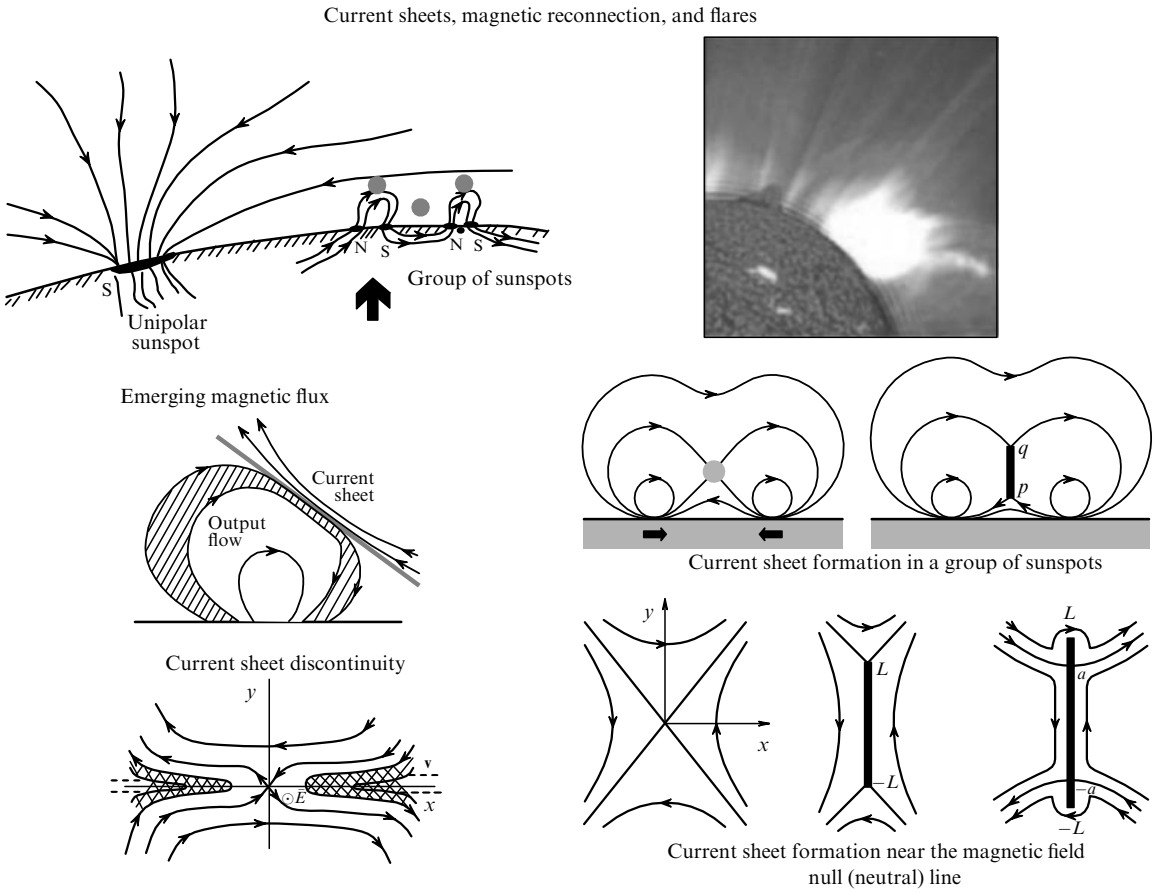

Figure 4. Illustrations of the theory of current sheets and solar flares developed by Syrovatskii.

craft [22, 23]. Their formation is related to the long-lived flare plasma confined by magnetic traps, and they are a manifestation of one of the coronal heating mechanisms, the conversion of magnetic energy into thermal energy in the flares (magnetic reconnection processes).

A statistical analysis of numerous observations according to spacecraft data (Yohkoh, SOHO, TRACE (Transition Region and Coronal Explorer), SMM (Solar Maximum Mission), etc.) showed that events with different energy releases (nanoflares, microflares, and ordinary flares) have common properties, expressed in a power-law distribution of the event number with respect to measured intensities [24]. There are many low-energy events and few high-energy ones. This result underlies the idea that the solar atmosphere is a system with developed turbulence down to very small scales, which sets conditions for dissipation. The role of turbulent vortices is played by reconnection processes at various scales.

5. Active phenomena and coronal heating

Among active solar atmospheric phenomena, the most powerful are solar flares and mass ejections. They are of major interest from both scientific and practical standpoints.

Syrovatskii made a fundamental contribution to the theory of solar flares and their adequate physical model [4]. According to Syrovatskii's theory, current sheets — high current concentrations — appear in the magnetic field structure near null points and neutral lines (Fig. 4). Free magnetic energy in the form of the current magnetic field energy is associated with this layer. It was demonstrated that this energy is sufficient for a flare to occur [25].

The flare itself is associated with the destruction of the current sheet due to various plasma instabilities [26], accompanied by magnetic reconnection in the sheet, a pulsed electric field appearing in the reconnection region, and particle acceleration by this field.

There have been attempts to identify pre-flare current sheets in the solar atmosphere based on their emission [27], in particular, radio emission [28, 29] characteristics. However, recent high-spatial-resolution space observations in the ultra-violet (UV) and X-ray ranges provided clear and demonstrative evidence of the existence of current sheets in solar active regions and their relation to solar flares, thus confirming the fundamentals of Syrovatskii's theory. In Fig. 5, an image obtained by the superposition of two SOHO (UV range, the structure of a magnetic field in the corona) and RHESSI (Reuven Ramaty High-Energy Solar Spectroscopic Imager) (X-ray range, nonthermal energy release) images demonstrates the formation of a current sheet in the solar atmosphere and an accompanying energy release during a flare.

As was already noted in Section 4, numerous magnetic reconnection events followed by ejections of two oppositely directed jets were found to be ubiquitous according to Hinode high-spatial-resolution observations [21]. Every increase in spatial resolution discloses new details of the small-scale solar atmospheric picture, the various forms of magnetic reconnection being one of its characteristic features. A large-scale rearrangement of the magnetic field structure in the solar corona was observed by CORONAS-F spacecraft [the SPIRIT (Russian for heliographic spectral investigations by

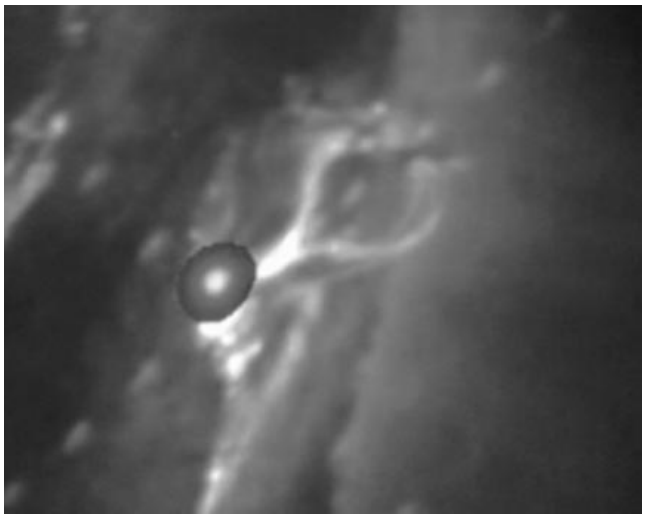

Figure 5. Superposed images of a solar flare illustrating the magnetic configuration with a current sheet (SOHO, UV radiation) and energy release in the flare associated with the sheet (RHESSI, hard X-rays).

an X-ray imaging telescope) experiment] during a very powerful flare on September 7, 2005 that occurred at the east limb [30]; this provided good visibility of the field structure. An initially closed loop field configuration became open after the flare, i.e., the field topology changed, thus indicating a magnetic reconnection.

In solar flares, charged particle acceleration occurs up to high energies (to a few dozen or hundred keV for electrons, and to 1–10 GeV for protons). In the current sheet theory, the initial charged-particle acceleration is related to strong pulsed electric fields that appear at the current sheet discontinuity and magnetic reconnection of field lines [26]. In the CORONAS-F spacecraft observations (the SPR-N experiment), the linear polarization of hard X-rays at the maximum of powerful solar flares was detected [31, 32]; this is related to bremsstrahlung in interactions of pulse-generated electron beams with the background plasma of the solar atmosphere [33]. These observations not only provide direct evidence of the existence of accelerated particle beams themselves, but also confirm that these particles are accelerated by the pulsed electric field during magnetic reconnection, and not by a stochastic mechanism.

RHESSI observations [34] gave answers to those flare physics questions that had previously been formulated and modeled in theoretical studies [33]. Together with TRACE observations, they allowed determining that energy release in flares in most cases occurs in loops and helmet-shaped configurations of plasma heated up to temperatures of a few tens of million degrees, as well as in the form of high-energy electrons moving downward from upper coronal layers and heating the plasma of lower layers. High-spatial-resolution observations of nonthermal X-rays (30–80 keV) allowed localizing the radiation source as the region of accelerated particle precipitation into dense layers of the solar atmosphere at the base of a magnetic loop, such that sources at different bases of the same loop have a different temporal profile and nonsimultaneous brightness increase.

Significant progress was achieved in the investigation of the most powerful phenomena of solar activity, the so-called coronal mass ejections observed in detail by SOHO, CORONAS-F, STEREO, and SDO. Most often, they have loop forms, and are typically twisted. Their origin is related to the global instability of a large-scale magnetic configuration [35].

In one of his last papers, Syrovatskii suggested a formation mechanism for the coronal mass ejection as the result of an outburst of the emerging magnetic flux into the corona [36]. A new emerging magnetic flux is accompanied by the appearance of a null point that moves upward with increasing the velocity, tending formally to infinity (taking the plasma into account, to the Alfvén speed). At some height, reconnection occurs at the null point, the magnetic field restructures, and a new magnetic flux via reconnection bursts out into the corona, leading to an ejection of mass together with the magnetic field (Fig. 6a). Later, with new observations taken into account, the model involving the null point and the current sheet as an inseparable part was detailed by other authors [37] (Fig. 6b), and this improved model soundly describes the actual picture of the ejection development and structure. The model of twisted loop ejections was proposed in Refs [38, 39].

6. Solar wind

The corona generates solar wind that continuously flows into the heliosphere. Local measurement on the Ulysses spacecraft allowed investigating the heliosphere above the ecliptic plane and studying the three-dimensional structure of the solar wind and the inner heliosphere, the magnetic field, the cosmic ray propagation in the heliosphere, and so on.

Figure 7 shows the helio-latitude dependence of the solar wind velocity, which for the minimum solar cycle phase showed a clear difference in the solar wind properties between the polar and equatorial regions: a high-speed (about 800 km s^{-1}) and stable solar wind from the polar regions and a low-speed (about 400 km s^{-1}) and variable solar wind from the near-equatorial regions [40]. For the maximum solar cycle phase, it is difficult to clearly distinguish between polar and equatorial regions according to the solar wind properties. The magnetic field topology distinctly affects the outflowing solar wind velocity. In polar regions, the field lines are mostly open and the wind speed is high here, whereas in near-equatorial regions, the closed field lines dominate and the wind speed is approximately two times lower. The twenty-third solar activity cycle (1995–2007) had maxima around 2000–2001, and two Ulysses spacecraft flights over the poles (north and south poles, at the distance 2 a.u.) were in the solar cycle maximum, and three were over the cycle minimum (two over the north pole and one over the south pole).

The question of solar wind sources on the Sun remains unexplained. In a recent model, it is assumed that the solar wind is formed along the boundaries (where the outflowing velocity is from 5 to 12 km s^{-1}) and at points (where the outflowing velocity is from 10 to 20 km s^{-1}) of the chromospheric magnetic network [41, 42] (Fig. 8). The solar wind plasma is delivered to the cell boundaries by closed magnetic loops dragged by convection in the funnel (magnetic tunnel) — regions of open field lines where they reconnect with the existing open magnetic field lines. The plasma initially stored inside the closed loops is released and accelerated, thus forming the solar wind. High-spatial-resolution observations of the Sun at short distances that are planned for future solar space missions (Interhelioprobe, Solar Orbiter, Solar Probe+) will allow answering the

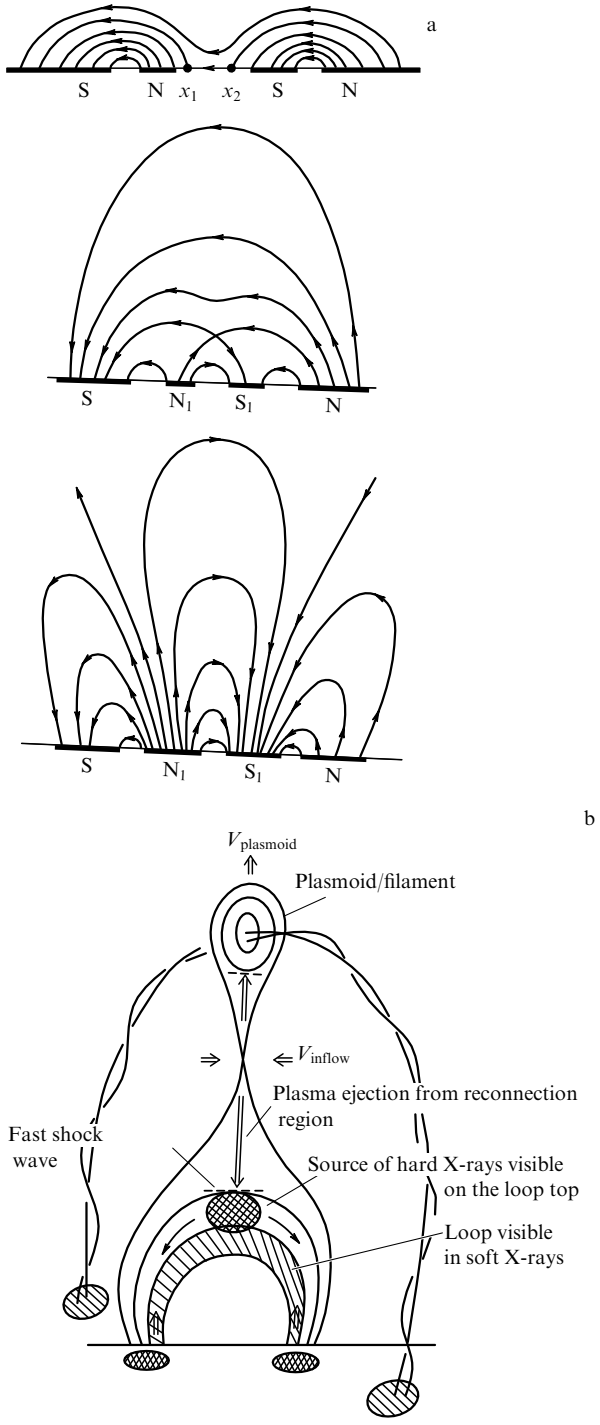

Figure 6. (a) Syrovatskii's ejection model based on an emerging new magnetic flux and its outburst into the corona as a result of magnetic reconnection at the null point [36]; x_1 and x_2 are the positions of the null points on the photosphere, S, S_1, N, and N_1 are the south and north polarities on the photosphere. (b) Development of the ejection model [37] on the basis of current observations (XR denotes X-ray radiation).

question regarding the true picture of solar wind sources on the Sun.

7. Space weather and its terrestrial effects

The Sun is the main source of space weather formation. Flares, mass ejections, and solar wind flows disturb the heliosphere and near-Earth space, causing magnetic storms and the accompanying phenomena [43]. In the STEREO

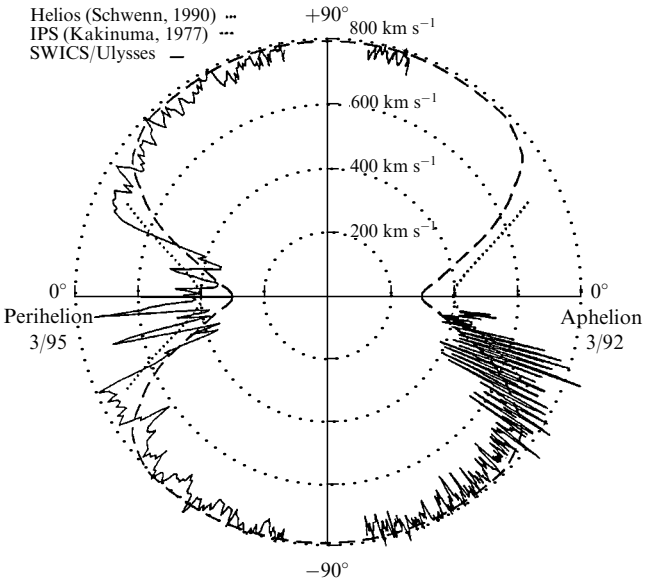

Figure 7. The helio-latitude dependence of the solar wind velocity obtained by the Ulysses spacecraft.

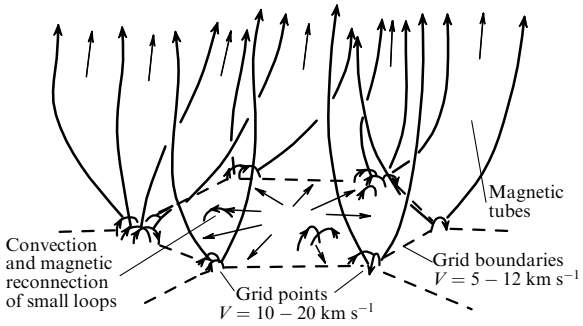

Figure 8. Magnetic network as a possible formation source of solar wind flows [41, 42].

project, two spacecraft rotate around the Sun in the terrestrial orbit, one of them ahead of Earth and the other at the same distance behind it, such that they can see a noticeable part of the Sun's back side and predict what activity we can expect on the visible side of the Sun. The overlapping of visual fields from these two spacecraft allowed creating stereo images and stereo films of the Sun, providing a 3D picture (Fig. 9). On the STEREO spacecraft, observations of mass ejections propagating from the Sun through the heliosphere were realized for the first time by using a heliospheric telescope [44]. These observations have allowed following the forefront motion of the ejection up to significantly larger distances compared to those provided by ordinary coronographs. The aim of these observations is to control the forefront collision with Earth's magnetosphere; this allows predicting the beginning of a geomagnetic storm and the related effects more accurately compared to current predictions.

Investigation of numerous space weather effects in the near-Earth space is related to practical applications of solar studies and solar–terrestrial physics. The space weather factors (ionospheric and geomagnetic field disturbances, enhanced fluxes of energetic particles and radiations, and so on) affect satellites, their electronics and drag, and ground-based technical systems (transmission lines and energy

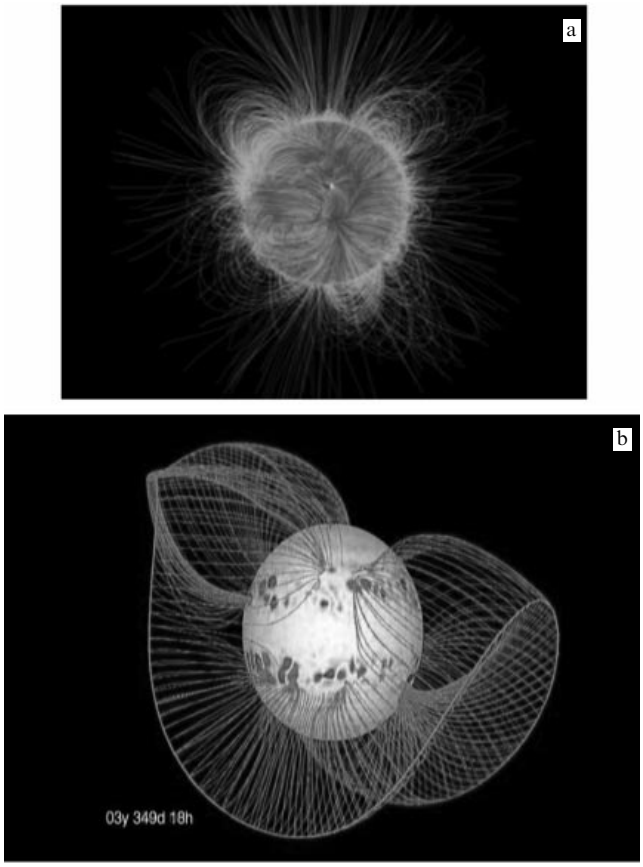

Figure 9. Three-dimensional magnetic fields (a) on the Sun and (b) in the heliosphere (heliospheric current layer) (modeling results by the SOHO scientific group).

infrastructure, pipelines, and so on). Space weather now is a vast research area [45].

8. Future solar space projects

The strategy of future solar space missions is to carry out observations with a higher spatial and temporal resolution, to conduct local measurements in the nearest solar environment, to obtain spectroscopic images from higher helio-latitudes, to make observations outside the Sun–Earth line, and to obtain 3D solar images. All these observation types are designed to improve our understanding of the phenomena occurring on the Sun and to explain unsolved problems of the Sun's physics such as solar coronal heating and solar wind acceleration, the nature of solar wind sources on the Sun's surface, trigger mechanisms of flares and mass ejections, the solar dynamo, and solar cycle mechanisms. Solving these problems will open the way to understanding the Sun's workings and the mechanism of solar–terrestrial connections, and will facilitate improvement of space weather forecasts and reduce the dependence of terrestrial civilization on space weather factors.

The time frames of space projects are important in the context of the phase of the 11-year solar activity cycle. The 23rd solar cycle finished in December 2008, and the 24th cycle is unpredictably long delayed. Such a long minimum solar cycle phase, which has already lasted for more than three years, was not predicted by experts. This tells us that we still understand the Sun and its cyclicity insufficiently well. The new cycle, with the maximum expected in 2012–2014, is predicted to not be high, and this prognosis will serve as an estimate of how correct our views of the Sun's workings are.

In the Russian Interhelioprobe Project [7, 46], which is currently being developed in the framework of the Federal Space Program, spacecraft will approach the Sun as a result of multiple gravitational maneuvering near Venus. Reaching of the corotation point is possible, when spacecraft will hover shortly above the Sun without relative motion. The near-Venus gravitational maneuvers will allow inclining the orbit plane with respect to the ecliptic plane, and performing out-of-ecliptic solar observations. The spacecraft approach to the Sun along the heliocentric orbit will make it possible to observe scales on the Sun smaller than those accessible from near-Earth orbits, which have only been used until now for space solar observations. This is necessary, for example, for investigating the fine structure and dynamics of the solar atmosphere: magnetic network, magnetic elements, and turbulence, as well as for observations of solar wind sources and phenomena such as microreconnection. The corotation regime observations will allow establishing relations between solar and heliospheric phenomena. Local measurements near the Sun, at distances of 40–60 solar radii, will allow investigating plasma processes in detail.

Looking further ahead, the Polar–Ecliptic Patrol (PEP) project is being worked out [7]; in this framework, two spacecraft at heliocentric inclined orbits around the Sun will proceed with a global solar survey and continuous observations of the Sun–Earth line from an out-of-ecliptic position, which should provide better understanding of the 3D picture of solar activity and near-solar space, and the most effective control of space weather.

9. Conclusion

In celebrating Syrovatskii's fruitful contribution to particular areas of solar physics, we stress that many of his ideas regarding the current sheet theory and the solar flare mechanism were confirmed by the results of solar space observations, which were in fact planned under the influence of Syrovatskii's work. The theory of current sheets and magnetic reconnection was significantly developed and observationally confirmed on the Sun, as well as in Earth's magnetosphere [47, 48]. In 2000, the first book on magnetic reconnection was published [47], which was then was translated into Russian. National solar space projects CORONAS-I, CORONAS-F, and CORONAS-FOTON have been realized. The CORONAS-F project work was honored with the Russian Federation Government Award (2008); the project results are presented in book [49]. Noticeable advances are being made in laboratory and numerical modeling of magnetic reconnection [50, 51]. Promising new national projects such as Interhelioprobe and Polar–Ecliptic Patrol are being developed. Continuing solar observations from space under the SOHO, TRACE, RHESSI, Hinode, STEREO, and SDO projects will provide a large amount of more detailed information on solar phenomena at the initial phase of the new cycle and improve understanding of processes occurring in our star.

References

1. Syrovatskii S I, in *Neitral'nye Tokovye Sloi v Plazme* (Neutral Current Sheets in Plasmas) (Proc. (Trudy) of the P N Lebedev Phys. Inst., Vol. 74, Ed. N G Basov) (Moscow: Nauka, 1974) p. 3 [Translated into English (New York: Consultants Bureau, 1976) p. 3]

2. Syrovatskii S I, in *Vspyshechnye Protsessy v Plazme* (Flares in Plasma) (Trudy FIAN, Vol. 110) (Moscow: Nauka, 1979) p. 5
3. Syrovatskii S I *Usp. Fiz. Nauk* **118** 738 (1976) [*Sov. Phys. Usp.* **19** 354 (1976)]
4. Syrovatskii S I *Solar Phys.* **53** 247 (1977)
5. Kuznetsov V D, in *Pyat'desyat Let Kosmicheskikh Issledovanii: po Materialam Mezhdunar. Foruma "Kosmos: Nauka i Problemy XXI Veka", Oktyabr' 2007, Moscow* (Fifty Years of Space Research: the International Forum "Cosmos. The Science and the Problems of the 21st Century", October 2007, Moscow) (Ed. A V Zakharov) (Moscow: Fizmatlit, 2009) p. 60
6. Kuznetsov V D *Usp. Fiz. Nauk* **180** 554 (2010) [*Phys. Usp.* **53** 528 (2010)]
7. Kuznetsov V D, Zelenyi L M, in *Solnechno-Zemnaya Fizika* (Solar-Terrestrial Physics) Issue 12 *Trudy Mezhdunar. Simpoziuma "Mezhdunarodnyi Geliofizicheskii God — 2007: Novyi Vzglyad na Solnechno-Zemnuyu Fiziku", Zvenigorod, 5–11 Noyabrya 2007 g.* (Proc. Intern. Symp. "International Heliophysical Year — 2007: New Glance at Solar-Terrestrial Physics", Zvenigorod, 5 – 11 November, 2007) Vol. 1 (Novosibirsk: Inst. Solnechno-Zemnoi Fiziki RAN, 2008) p. 83
8. Christensen-Dalsgaard J "Lecture notes on stellar oscillations," http://www.phys.au.dk/~jcd/oscilnotes/
9. Lebedev N I et al. *Astron. Zh.* **81** 956 (2004) [*Astron. Rep.* **48** 871 (2004)]
10. Zhugzhda Yu D, Kuznetsov V D, Lebedev N I, in *Solnechno-Zemnaya Fizika: Rezul'taty Eksperimentov na Sputnike KORONAS-F* (Solar–Terrestrial Physics: The Results of Experiments on Board the CORONAS-F Satellite) (Ed. V D Kuznetsov) (Moscow: Fizmatlit, 2009) p. 35
11. Kosovichev A G, Duvall T L, Scherrer P H *Solar Phys.* **192** 159 (2000)
12. Lindsey C, Braun D C *Science* **287** 1799 (2000)
13. Parker E N *Astrophys. J.* **138** 552 (1963)
14. Parker E N *Astrophys. J.* **221** 368 (1978)
15. Nagata S et al. *Astrophys. J.* **677** L145 (2008)
16. Katsukawa Y et al. *Science* **318** 1594 (2007)
17. Parnell C E *Solar Phys.* **200** 23 (2001)
18. Erdélyi R, Fedun V *Science* **318** 1572 (2007)
19. Cirtain J W et al. *Science* **318** 1580 (2007)
20. Parker E N *Astrophys. J.* **330** 474 (1988)
21. Shibata K et al. *Science* **318** 1591 (2007)
22. Bogachev S A et al. *Astron. Vestn.* **39** 571 (2005) [*Solar Syst. Res.* **39** 508 (2005)]
23. Zhitnik I A et al., in *Solnechno-Zemnaya Fizika: Rezul'taty Eksperimentov na Sputnike KORONAS-F* (Solar–Terrestrial Physics: The Results of Experiments on Board the CORONAS-F Satellite) (Ed. V D Kuznetsov) (Moscow: Fizmatlit, 2009) p. 65
24. Aschwanden M J et al. *Astrophys. J.* **535** 1047 (2000)
25. Syrovatskii S I *Pis'ma Astron. Zh.* **2** 35 (1976) [*Sov. Astron. Lett.* **2** 13 (1976)]
26. Syrovatskii S I, Bulanov S V, Dogel' V A, in *Itogi Nauki i Tekhniki* (Progress in Science and Technology) (Ser. Astronomy, Vol. 21) (Moscow: VINITI, 1982) p. 188
27. Syrovatskii S I *Pis'ma Astron. Zh.* **3** 133 (1977) [*Sov. Astron. Lett.* **3** 69 (1977)]
28. Kuznetsov V D, Syrovatskii S I *Solar Phys.* **69** 361 (1981)
29. Kuznetsov V D *Astron. Zh.* **59** 108 (1982) [*Sov. Astron.* **26** 67 (1982)]
30. Kuznetsov V D, in *Solnechno-Zemnaya Fizika: Rezul'taty Eksperimentov na Sputnike KORONAS-F* (Solar-Terrestrial Physics: Results of CORONAS-F Satellite-Borne Experiments) (Ed. V D Kuznetsov) (Moscow: Fizmatlit, 2009) p. 10
31. Zhitnik I A et al., in *Solnechno-Zemnaya Fizika: Rezul'taty Eksperimentov na Sputnike KORONAS-F* (Solar–Terrestrial Physics: The Results of Experiments on Board the CORONAS-F Satellite) (Ed. V D Kuznetsov) (Moscow: Fizmatlit, 2009) p. 128
32. Kuznetsov V D *Izv. Ross. Akad. Nauk Ser. Fiz.* **70** 56 (2006)
33. Syrovatskii S I, Somov B V, in *Itogi Nauki i Tekhniki* (Progress in Science and Technology) (Ser. Astronomy, Vol. 21) (Moscow: VINITI, 1982) p. 221
34. Lin R P et al. *Solar Phys.* **210** (1 – 2) 3 (2002), Special Issue: The Reuven Ramaty High-Energy Solar Spectroscopic Imager (RHESSI): Mission Description and Early Results
35. Kuznetsov V D, in *Plazmennaya Geliogeofizika* (Plasma Helio-Geophysics) Vol. 1 (Eds L M Zelenyi, I S Veselovskii) (Moscow: Fizmatlit, 2008) p. 81
36. Syrovatskii S I *Solar Phys.* **76** 3 (1982)
37. Shibata K et al. *Astrophys. J.* **451** L83 (1995)
38. Kuznetsov V D, Hood A W *Solar Phys.* **171** 61 (1997)
39. Kuznetsov V D, Hood A W *Adv. Space Res.* **26** 539 (2000)
40. McComas D J et al. *Gephys. Res. Lett.* **30** 1517 (2003)
41. Axford W I, McKenzie J F, in *Cosmic Winds and the Heliosphere* (Eds J R Jokipii, C P Sonett, M S Giampapa) (Tucson: Univ. of Arizona, 1997) p. 31
42. Hassler D M et al. *Science* **283** 810 (1999)
43. Kuznetsov V D *J. Atm. Solar-Terr. Phys.* **70** 234 (2008)
44. Harrisson R et al. *COSPAR's Inform. Bull.* **168** 25 (2007)
45. Bothmer V, Daglis I A *Space Weather: Physics and Effects* (Berlin: Springer, 2007)
46. Kuznetsov V D *Usp. Fiz. Nauk* **176** 319 (2006) [*Phys. Usp.* **49** 305 (2006)]
47. Priest E R, Forbes T *Magnetic Reconnection: MHD Theory and Applications* (Cambridge: Cambridge Univ. Press, 2000) [Translated into Russian (Moscow: Fizmatlit, 2005)]
48. Zelenyi L M *Usp. Fiz. Nauk* **180** 973 (2010) [*Phys. Usp.* **53** (2010)]
49. Kuznetsov V D (Ed.) *Solnechno-Zemnaya Fizika: Rezul'taty Eksperimentov na Sputnike KORONAS-F* (Solar-Terrestrial Physics: Results of CORONAS-F Satellite-Borne Experiments) (Moscow: Fizmatlit, 2009)
50. Frank A G *Usp. Fiz. Nauk* **180** 982 (2010) [*Phys. Usp.* **53** (2010)]
51. Yamada M, Kulsrud R, Ji H *Rev. Mod. Phys.* **82** 603 (2010)

PACS numbers: 52.30.Cv, 52.35.Vd, 96.60.qe
DOI: 10.3367/UFNe.0180.201009j.0997

Magnetic reconnection in solar flares

B V Somov

1. Introduction

I was privileged to work under the supervision of Sergei Ivanovich Syrovatskii from 1966 to 1979, first as a graduate and postgraduate student, and then as a scientist at the Theoretical Department of the Lebedev Physics Institute. During those years, which quickly flew by, Syrovatskii was mostly interested in the solar flare problem.

The essence of the problem, its scientific and applied value, is determined by two facts. First, solar flares are a nonstationary electromagnetic phenomenon, typical for space plasmas but accessible to the most detailed investigations, in contrast to other stellar flares and bursts of objects in the Universe. Second, solar flares strongly influence interplanetary and near-Earth space, Earth's atmosphere, and even the biosphere. It is no coincidence that solar flares are interesting for not only astronomers and physicists but also specialists in cosmonautics/astronautics and power engineering, as well as biologists and medics. Syrovatskii made a fundamental contribution to establishing and successfully developing theoretical and experimental solar flare science in our country and abroad. In this communication, I touch upon only one key issue of this science, the role of the

B V Somov Shternberg State Astronomical Institute,
Lomonosov Moscow State University,
Moscow, Russian Federation. E-mail: somov@sai.msu.ru

Uspekhi Fizicheskikh Nauk **180** (9) 997 – 1000 (2010)
DOI: 10.3367/UFNr.0180.201009j.0997
Translated by S V Vladimirov; edited by A M Semikhatov

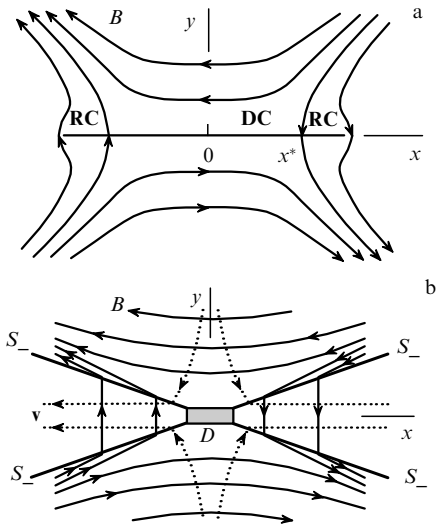

Figure 1. Two classic reconnection models: (a) the Syrovatskii current layer, and (b) the Petschek flow.

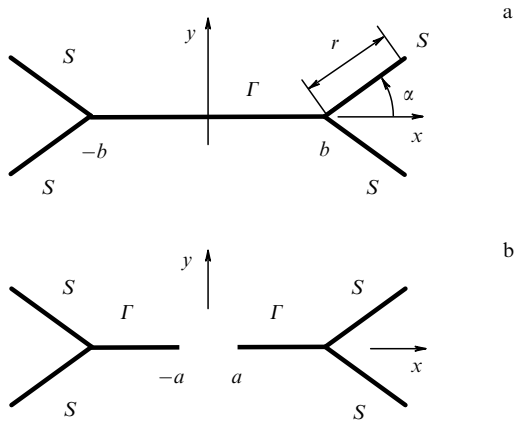

Figure 2. Current configuration containing a current layer Γ and four attached discontinuous MHD flows S with a finite width r: (a) the current layer without discontinuity, and (b) the current layer with a discontinuity of width $2a$.

magnetic field line reconnection (magnetic reconnection) in the flares [1, 2].

2. Syrovatskii's current layer

Magnetic reconnection is a redistribution of magnetic fluxes resulting in a change in the field topology. In both the medium and the vacuum, this process induces an electric field that is manifested depending on the medium properties. In the vacuum, for example, it can be merely measured or used to accelerate a charged particle. In plasma, the electric field generates an electric current; to be more precise, a current structure, which is typically fairly complex.

In a highly conducting plasma, the electric field forms a narrow current layer impeding redistribution of interacting magnetic fluxes [3, 4]. This leads to an energy excess in the form of the magnetic field in the current layer. The wider the layer is, the more energy is accumulated, and this is extensively used in astrophysical applications of the magnetic reconnection effect.

In a strong magnetic field, its structure near the current layer in a highly conducting plasma can be described by a simple analytic model [7], namely, as a discontinuity surface separating oppositely directed fields (Fig. 1a). This model is called the Syrovatskii current layer. The layer contains a direct current (DC) region and two attached reverse current (RC) regions. The magnetic field outside the current layer is considered to be potential, or more precisely, a two-dimensional field whose complex potential is an analytic function.

Another classic reconnection model, called the Petschek flow [8], is usually regarded as an alternative to the Syrovatskii current layer. In the Petschek model, the magnetic field line reconnection process is essentially separated from the field dissipation process. Reconnection occurs in a small diffusion region D (Fig. 1b). Energy release in this small region can be neglected, in contrast to the magnetic field energy that is converted into the plasma thermal and kinetic energy on four associated slow magnetohydrodynamic (MHD) shock waves S_- of infinite length.

3. Necessary generalizations of classic models

Already the first numerical simulations [9, 10] of the dissipative MHD magnetic reconnection have shown that there are finite-length discontinuous MHD flows near the current layer edges. The observed pattern of the flows is quite complex and, of course, depends on the initial and boundary conditions. Moreover, natural restrictions intrinsic for finite-difference methods do not allow investigating the current layer structure in the reconnection regime corresponding to the so-called super-hot turbulent current layers in solar flares [6]. The above conditions require that generalized analytic models should be constructed and reasonably simplified, and should explicitly depend on the physical parameters of the reconnection region. For solar flares, such parameters are, first of all, the geometric features of the region: a characteristic width b of the current layer, the angle α between the layer and the attached shock waves, and their length r (Fig. 2a).

The question of boundary and initial conditions in a general magnetic reconnection problem is not trivial. In the generalized model in [11, 12], as well as in Syrovatskii's model [7], the normal component of the magnetic field vanishes on the layer, i.e., the current layer is neutral. Accounting for a small transverse field component related to the reconnection process inside the layer is generally necessary and possible; however, that complicates the problem significantly. Taking the current layer symmetry into account, the problem can be reduced to a mixed Riemann–Hilbert boundary value problem [13] (see also Section 3.4 in Ref. [14], where a particular solution in the framework of the Keldysh–Sedov problem [13] is given). The transverse component of MHD shock waves is equal to a given constant β. This last assumption somewhat restricts the class of possible solutions; but it is necessary to limit the complexity regarding the formulation of the mathematical problem.

Another generalization of Syrovatskii's model is necessary in relation to the narrow layer decay into parallel current ribbons. Such a layer tearing can occur as a result of the tearing instability or when a higher resistivity occurs in the layer region, for example, anomalous resistivity owing to the excitation of some plasma turbulence. A simple analytic model of a decaying layer of infinite width was suggested in Ref. [15]. The magnetic tension force acts on the discontinuity sides in the layer; the force is proportional to the discontinuity width and tends to widen it. A powerful electric field is

induced inside the discontinuity; in astrophysical conditions (e.g., in solar flares), this field is capable of accelerating charged particles to high energies. A generalized problem for a finite-width current layer in the presence of attached discontinuous flows, taking the current layer discontinuity into account, was formulated and solved in Ref. [16].

4. New analytic models

The generalized model described in Section 3 assumes that the two-dimensional magnetic field is potential in the region g outside the current configuration represented by a set of cuts $\Gamma + 4S$ on the complex plane $z = x + \mathrm{i}y$ (see Fig. 2). The magnetic field itself is also written in the complex form

$$B(z) = B_x(x, y) + \mathrm{i}B_y(x, y)\,. \tag{1}$$

The field component B_n normal to the line $\Gamma + 4S$ vanishes on the current layer Γ, and is equal to a given constant β on the cuts S corresponding to shock waves. Herewith, B_n is expressed in terms of B as

$$B_n = \mathrm{Re}\left[v(z)\,\bar{B}(z)\right], \tag{2}$$

where $v(z)$ is the complex unit normal, Re is the real part of the quantity in square brackets, and the bar over B denotes complex conjugation.

At infinity, the function $B(z)$ satisfies the condition

$$B(x, y) \sim \mathrm{i}h\,\bar{z}\,, \qquad z \to \infty\,, \tag{3}$$

where h is the magnetic field gradient. Such behavior of the field corresponds to the pattern of lines observed far away from the hyperbolic null point in Syrovatskii's model [7].

To find the magnetic field function B, it is convenient to use its complex conjugate,

$$\mathcal{F}(z) = u(x, y) + \mathrm{i}v(x, y) = \bar{B}(z)\,, \qquad z \in g\,, \tag{4}$$

because it follows from the potential character of the field that the function $\mathcal{F}(z)$ defined this way is an analytic function of the complex variable z in region g. Replacing B with $\bar{\mathcal{F}}$ in (2) and taking the boundary conditions on the $\Gamma + 4S$ cuts into account, we obtain the Riemann–Hilbert problem for $\mathcal{F}(z)$:

$$\mathrm{Re}\left[v(z)\mathcal{F}(z)\right] = c(z) \quad \text{on} \quad \Gamma + 4S\,. \tag{5}$$

Here, $c(z)$ is a known function: $c(z) = 0$ on the current layer Γ and $c(z) = \beta$ on the cuts S.

Figure 3 illustrates the problem solution method [17]. Because the problem is symmetric with respect to the x and y axes, it is sufficient to consider one quarter of region g, e.g., the first quadrant with cut CDE, the region G (Fig. 3a). Because region G is an infinite pentagon, it can be mapped on the upper half-plane $\mathbb{H}^+$ (Fig. 3b) by using a conformal map $\zeta = \Phi(z)$ whose inverse can be represented as the Christoffel–Schwarz integral [18]

$$\Phi^{-1}(\zeta) = \mathscr{K} \int_0^{\zeta} t^{-1/2}(t - \lambda)^{-\alpha}(t - 1)\,(t - \tau)^{\alpha - 1}\,\mathrm{d}t\,. \tag{6}$$

The problem solution $\mathscr{P}(\zeta)$ in the upper half-plane $\mathbb{H}^+$ can be obtained by standard methods [13]; it is shown in Fig. 3c. Substituting $\zeta = \Phi(z)$ in $\mathscr{P}(\zeta)$, we finally write the general solution $\mathcal{F}$ in the form $\mathcal{F}(z) = \mathscr{P}[\Phi(z)]$.

An analytic solution of the problem of a current layer with attached shock waves (Fig. 4) was obtained in Ref. [12]. The

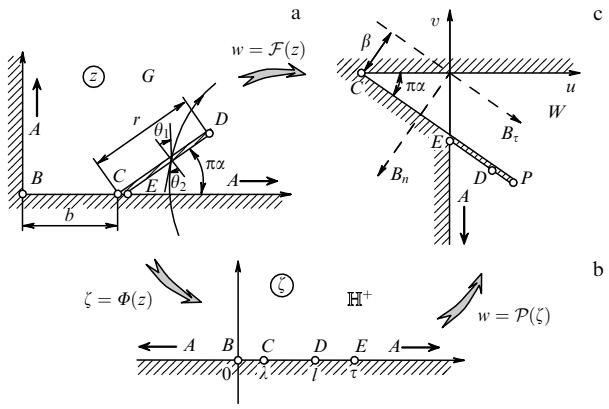

Figure 3. Sketch to solve the Riemann–Hilbert problem. (a) Initial region. (b) Upper half-plane. (c) Magnetic field locus region.

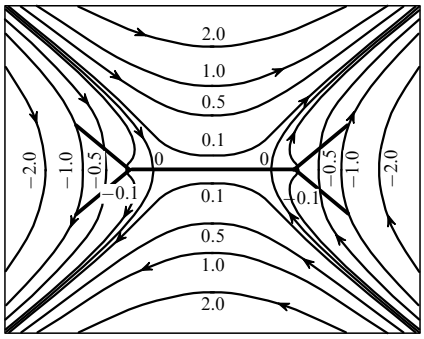

Figure 4. Current structure (bold straight line segments) and magnetic field lines (thin curves, with arrows showing the field direction) in the model of a current layer with attached shock waves [12] for characteristic parameter values $b = r = 1$, $\alpha = 1/4$, $\beta = 1$, and $h = 1$.

model allowed studying a global arrangement of the magnetic field and the behavior of the total current and reconnection rate determined by the magnetic field as functions of the parameters β and h. The character of the magnetic field refraction on the shock wave, i.e., on cut CDE (Fig. 3a), was considered in Ref. [16].

We let θ_1 and θ_2 be the respective deviation angles of the magnetic field vector from the interior (with respect to region G) normals to boundary segments CD and DE. The ratio of these two angles determines the MHD wave type (see Ref. [19]). For example, if both angles are positive and $\theta_2 > \theta_1$, the wave is fast, and in the case $\theta_1 > \theta_2$, slow. As demonstrated in Ref. [16], near the attachment point of a shock wave to a current layer, there is always a segment of cut S where the wave is a trans-Alfvénic shock. It increases the tangential field component and changes its direction to the opposite (see Ref. [20]). Trans-Alfvénic waves are non-evolutionary (see Ref. [19]). The analysis of the evolutionary character of a current layer itself (see Ch. 10 in Ref. [6]) has shown that in reverse-current regions, the layer, as an MHD discontinuity, is not evolutionary [21] and can therefore split into other discontinuities observed in the numerical simulations in [22, 23]. Figure 5 shows the magnetic field pattern for the model with a decaying current layer in the presence of attached shock waves (Fig. 2b). Clearly seen are the direct and reverse current regions, and the field line refraction on shock waves.

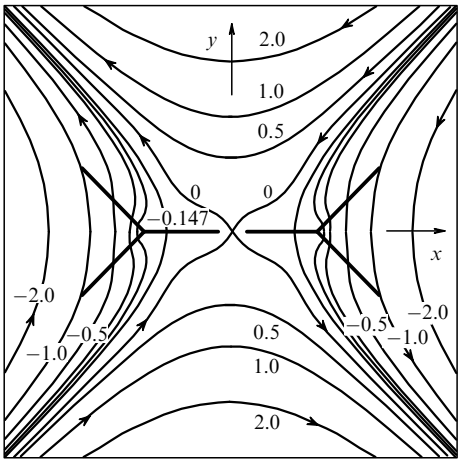

Figure 5. Pattern of magnetic field lines near a decaying current layer with attached shock waves [16].

5. The physics of reconnecting current layers

In space and laboratory plasmas, the magnetic reconnection effect underlies many nonstationary phenomena accompanied by fast plasma flows and shock waves, powerful heat fluxes, and fluxes of charged particles accelerated to high energies. Among these phenomena are, first of all, solar flares accessible for comprehensive investigation and detailed modeling [24]. On the Sun, reconnecting current layers naturally appear in the corona, in the magnetic fields of the so-called active regions, where magnetic fields are strong and the reconnecting current layer electric fields reach enormous values.

The analytic models considered above do not describe physical processes inside a current layer. In the strong-field approximation, a current layer is an infinitely thin MHD discontinuity. Due to the two-dimensional character of the reconnection effect, such a discontinuity essentially differs from one-dimensional MHD discontinuities included in the standard classification [25]. The field structure in its vicinity is described by Syrovatskii's solution [7]. The plasma dynamics near a current layer can be investigated in the same approximation (see Ch. 3 in Ref. [26]). In particular, it is possible to find velocities of plasma flows together with the frozen magnetic field and identify the inflow velocity in the layer with the reconnection rate in it. Thus, Syrovatskii's solution, describing the two-dimensional magnetic field structure near a current layer, plays the same role as the Hugoniot adiabate that determines parameters of a stationary one-dimensional gas flow through a hydrodynamic shock wave front. The corresponding MHD generalizations of the Hugoniot adiabate are applicable to MHD shock waves attached to a current layer.

In the framework of the above models, the parameters of a current layer and shock waves are considered fixed. In specific astrophysical applications, for example, solar flares, a particular physical model should be used to determine these parameters (such as the current layer half-width b), namely, the high-temperature turbulent current layer model (the shaded oval area in Fig. 6) (see Ch. 6 in Ref. [6]). This two-dimensional self-consistent model is based on the mass, momentum, and energy conservation laws (as well as on Ohm's law) written as order relations.

The temperature of the current layer is so high that Coulomb collisions can be neglected there. Direct heating of

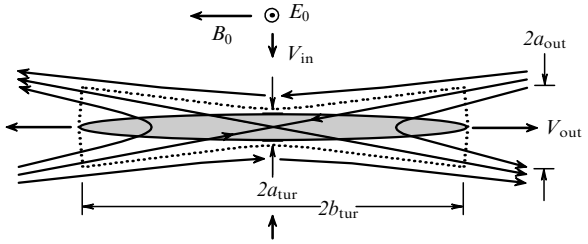

Figure 6. A high-temperature turbulent current layer [6] as a physical model of the direct current region in a reconnecting current layer.

electrons and ions as a result of particle–wave interactions inside the turbulent layer and the electron cooling by anomalous thermal fluxes from the layer are the dominant physical processes in such a 'super-hot' layer [27, 28]. The model allows estimating characteristic values of the turbulent layer thickness $2a_{tur}$ and width $2b_{tur}$ (see Fig. 6), the plasma density, the electron and ion temperature in it, and the energy release power and other parameters that are interesting for astrophysical applications of the magnetic reconnection theory.

However, a significant advantage of analytic models is the possibility of investigating general relations independent of detailed assumptions regarding the physical reconnection model in strong magnetic fields. This is highly analogous to the Hugoniot adiabate, which describes the initial and final gas state at its transition through a shock wave front irrespective of how exactly the transition occurs.

References

1. Syrovatskii S I *Astron. Zh.* **39** 987 (1962) [*Sov. Astron.* **6** 768 (1963)]
2. Syrovatskii S I *Solar Phys.* **76** 3 (1982)
3. Syrovatskii S I *Zh. Eksp. Teor. Fiz.* **50** 1133 (1966) [*Sov. Phys. JETP* **23** 754 (1966)]
4. Imshennik V S, Syrovatskii S I *Zh. Eksp. Teor. Fiz.* **52** 990 (1967) [*Sov. Phys. JETP* **25** 656 (1967)]
5. Somov B V, Syrovatskii S I *Usp. Fiz. Nauk* **120** 217 (1976) [*Sov. Phys. Usp.* **19** 813 (1976)]
6. Somov B V *Plasma Astrophysics* Pt. II *Reconnection and Flares* (New York: Springer, 2006)
7. Syrovatskii S I *Zh. Eksp. Teor. Fiz.* **60** 1727 (1971) [*Sov. Phys. JETP* **33** 933 (1971)]
8. Petschek H E, in *The Physics of Solar Flares, Proc. of the AAS–NASA Symp., 28–30 October, 1963, Greenbelt, MD* (Ed. W N Hess) (Washington, DC: NASA, 1964) p. 425
9. Brushlinskii K V, Zaborov A M, Syrovatskii S I *Fiz. Plazmy* **6** 297 (1980) [*Sov. J. Plasma Phys.* **6** 165 (1980)]
10. Biskamp D *Phys. Fluids* **29** 1520 (1986)
11. Markovskii S A, Somov B V, in *Fizika Solnechnoi Plazmy* (Physics of the Solar Plasma) (Eds B V Somov, V V Fomichev) (Moscow: Nauka, 1989) p. 45
12. Bezrodnykh S I, Vlasov V I, Somov B V *Pis'ma Astron. Zh.* **33** 153 (2007) [*Astron. Lett.* **33** 130 (2007)]
13. Lavrent'ev M A, Shabat B V *Metody Teorii Funktsii Kompleksnogo Peremennogo* (Methods of the Theory of Complex-Variable Functions) (Moscow: Nauka, 1973)
14. Somov B V *Physical Processes in Solar Flares* (Dordrecht: Kluwer Acad. Publ., 1992)
15. Somov B V, Syrovatskii S I *Izv. Akad. Nauk SSSR Ser. Fiz.* **39** 375 (1975) [*Bull. Acad. Sci. USSR Phys. Ser.* **39** (2) 109 (1975)]
16. Bezrodnykh S I, Vlasov V I, Somov B V *Pis'ma Astron. Zh.* **36** (10) (2010) [*Astron. Lett.* **36** (10) (2010)]
17. Bezrodnykh S I, Vlasov V I *Zh. Vychisl. Mat. Mat. Fiz.* **42** 277 (2002) [*Comput. Math. Math. Phys.* **42** 263 (2002)]

18. von Koppenfels W, Stallmann F *Praxis der Konformen Abbildung* (Berlin: Springer, 1959) [Translated into Russian (Moscow: IL, 1963)]
19. Somov B V *Plasma Astrophysics* Pt. I *Fundamentals and Practice* (New York: Springer, 2006)
20. Ledentsov L S, Somov B V *Pis'ma Astron. Zh.* **36** (10) (2010) [*Astron. Lett.* **36** (10) (2010)]
21. Markovskii S A, Somov B V *J. Plasma Phys.* **55** 303 (1996)
22. Chen P F et al. *Astrophys. J.* **513** 516 (1999)
23. Ugai M *Phys. Plasmas* **15** 082306 (2008)
24. Somov B V et al. *Adv. Space Res.* **32** 2439 (2003)
25. Syrovatskii S I *Usp. Fiz. Nauk* **62** 247 (1957)
26. Somov B V, Syrovatskii S I, in *Neitral'nye Tokovye Sloi v Plazme* (Neutral Current Sheets in Plasmas) (Proc. (Trudy) of the P N Lebedev Phys. Inst., Vol. 74, Ed. N G Basov) (Moscow: Nauka, 1974) p. 14 [Translated into English (New York: Consultants Bureau, 1976) p. 13]
27. Somov B V, Titov V S *Pis'ma Astron. Zh.* **9** 48 (1983) [*Sov. Astron. Lett.* **9** 26 (1983)]
28. Oreshina A V, Somov B V *Pis'ma Astron. Zh.* **26** 870 (2000) [*Astron. Lett.* **26** 750 (2000)]

PACS numbers: 96.50.S–, 97.60.Bw, 98.62.Nx
DOI: 10.3367/UFNe.0180.201009k.1000

The origin of cosmic rays

V S Ptuskin

1. Introduction

Cosmic ray studies constitute an important part of Sergei Ivanovich Syrovatskii's scientific heritage. The famous book published in 1963 by Ginzburg and Syrovatskii, *The Origin of Cosmic Rays* [1], has become a 'Bible' for scientists working in high-energy astrophysics. Already in this book, which was written before the discovery of quasars, cosmic background radiation, and pulsars, during the days when information on cosmic rays beyond the Solar System was based primarily on radio astronomy data, the foundations of the cosmic ray origin model were formulated, which remain firm up to this day. The model developed in Ref. [1] is based on the following assumptions: the main component of cosmic rays is of galactic origin, the cosmic rays diffuse in interstellar magnetic fields and fill a vast halo, the cosmic ray sources are supernova explosions, and the highest-energy particles (according to the modern nomenclature, cosmic rays with energies above $10^{18}-10^{19}$ eV) have an extragalactic origin. In 1979, shortly after Syrovatskii's death, Ginzburg suggested to several colleagues working in this field to jointly write a book on this topic. The book *Astrophysics of Comic Rays*, edited by Ginzburg, was published in 1984, and a second edition appeared in 1990. It included new chapters such as gamma-ray and neutrino astronomy, and a kinetic description of cosmic ray acceleration and propagation processes. In a certain sense, that book was a comprehensive summary of many years of collaborative work of Ginzburg, Syrovatskii, and their colleagues in the field of cosmic ray astrophysics.

In this brief communication, we describe, some recent results of research into the origin of cosmic rays.

V S Ptuskin Pushkov Institute of Terrestrial Magnetism, Ionosphere, and Radio Wave Propagation, Russian Academy of Sciences, Troitsk, Moscow region, Russian Federation. E-mail: vptuskin@izmiran.ru

Uspekhi Fizicheskikh Nauk **180** (9) 1000 – 1004 (2010)
DOI: 10.3367/UFNr.0180.201009k.1000
Translated by S V Vladimirov; edited by A M Semikhatov

2. Galactic cosmic rays: acceleration in supernovae and propagation in galactic magnetic fields

Because of their energy characteristics, supernovae and their remnants are the most suitable galactic cosmic ray sources [1]. To obtain the observed energy density of cosmic rays, ≈ 1.5 eV cm^{-3}, approximately 10–20% of the kinetic energy of a supernova burst should be converted into the energy of relativistic particles. It is assumed that the kinetic energy of a supernova explosion is 10^{51} erg and that galactic supernova outbursts occur every 30 years on average. Direct evidence of the presence of relativistic particles in supernova remnants follow from nonthermal radiation observations in the radio, X-ray, and gamma-ray ranges. Synchrotron radio emission data indicate that there are electrons with energies 50 MeV–30 GeV in supernova remnants such as Cas A, IC 433, Cygnus Loop, and many others [3]. In the case of Cas A, the synchrotron radiation was detected in the infrared range, which indicates that there are electrons with energies up to 200 GeV. The nonthermal X-ray radiation with a characteristic power-law spectrum and energy up to a few dozen keV detected from bright rims in approximately ten young galactic supernova remnants, including SN1006, Cas A, RXJ 1713.7-3946, RX J08852-46/Vela Jr, RCW86, and G266.2-1.2 can be explained by synchrotron emission of very-high-energy electrons, up to 10–100 TeV (see review [4]). The inverse Compton scattering of background photons by such high-energy electrons, and gamma-ray emission via π^0-meson production and decays in interaction processes of protons and nuclei with energies up to ~ 100 TeV with gas nuclei, explain the presence of TeV gamma emissions detected from a number of young shell-type supernova remnants [5]. Spatial distribution of nonthermal emission in all frequency ranges demonstrates that particle acceleration occurs directly on the shock wave produced by the supernova explosion.

Cosmic ray composition data also confirm that particle acceleration occurs on a shock wave propagating in the interstellar medium or presupernova wind (see [6] for the details). In particular, it turns out that after accounting for the atomic properties such as the first ionization potential or volatility (the composition of matter deposited on the interstellar dust is volatility dependent), the chemical composition of cosmic ray sources is close to the typical composition of the local interstellar medium or solar photosphere. The ion and dust acceleration probably occurs in the partially ionized interstellar gas and/or hot interstellar gas bubbles with a high rate of supernova outbursts. The relatively high abundance ratio of ^{59}Co/^{56}Fe isotopes in the material of cosmic ray sources shows that most ^{59}Ni isotopes synthesized in a supernova explosion have time to decay into ^{59}Co isotopes due to orbital electron capture before the particle acceleration begins. It therefore follows that the acceleration occurs no less than 10^5 years after the nucleosynthesis process.

The mechanism of cosmic ray acceleration in supernova remnants is a version of the first-order Fermi acceleration. Acceleration of fast particles occurs in a gas flow that is compressed on the shock wave owing to multiple shock wave front crossings by diffusing fast particles [7, 8] (see also

reviews [6, 9]). The particle diffusion is due to their scattering on magnetic field inhomogeneities. This scattering has a resonant character, and therefore a particle with a gyroradius r_g mostly interacts with inhomogeneities with the wavenumber $k \sim 1/r_g$. The particle diffusion coefficient can be estimated as $D \approx v r_g B^2 (3B_{res}^2)^{-1}$, where v is the particle velocity, B is the total magnetic field, and B_{res} is the random magnetic field at the resonant scale $1/k \sim r_g$. The momentum distribution function of accelerated particles has a power-law character, $f(p) \propto p^{-3r/(r-1)}$, where r is the gas compression ratio on the shock wave (the function $f(p)$ is related to the cosmic ray intensity $I(E)$ as $p^2 f(p) = I(E)$, where E is the particle energy). The ultimate gas compression in a strong shock wave propagating in a monatomic gas without luminescence is $r = 4$, which for ultrarelativistic energies results in the accelerated particle spectrum $I(E) \sim E^{-2}$. This applies to the test-particle acceleration. For effective acceleration on a shock wave produced by a supernova explosion, the relativistic particle pressure becomes so strong that the shock wave profile is modified and the emerging self-consistent spectrum of accelerated particles essentially differs from that of test particles: it steepens for nonrelativistic energies and can flatten to $\sim E^{-3/2}$ in the highest energy range.

The necessary condition for acceleration is the inequality $D \leqslant 0.1 u_{sh} R_{sh}$, where u_{sh} and R_{sh} are the shock wave velocity and radius, and the numerical factor 0.1 is calculated approximately. The expression in the right-hand side of this inequality reaches the maximum value $\sim 10^{27} (W_{51}/n)^{2/5}$ [cm^2 s^{-1}] at the beginning of the Sedov phase of supernova remnant evolution; here, the supernova explosion energy is $W_{sn} = 10^{51} W_{51}$ [erg], and n is the interstellar gas number density in cm^{-3}. But the typical value of the galactic cosmic ray diffusion coefficient is $D_G \sim 10^{28}$ cm^2 s^{-1} for the particle energy 1 GeV per nucleon, increasing as the energy increases; this becomes too large to ensure the relativistic particle acceleration. Therefore, an anomalously low diffusion is necessary near the shock wave front, including the region directly before the front. This is ensured by the accelerated particles themselves that leave the acceleration region and create an enhanced level of magnetohydrodynamic (MHD) turbulence owing to the streaming instability. The weak turbulence theory predicts a significant amplification of the random magnetic field δB for shock waves with a large Mach number; but the theory cannot adequately describe the field increase up to a value comparable with the background interstellar magnetic field $B_0 = 5$ μG. Assuming that $\delta B = B_0$, we can obtain the so-called Bohm diffusion coefficient $D_{B0} = v r_g/3 \sim 6 \times 10^{21} \beta R_m$ [cm^2 s^{-1}] that is the low limit for the particle diffusion coefficient along the magnetic field (here, $\beta = v/c$, and $R_m = pc/Z$ is the magnetic rigidity for a particle with the charge Z). The Bohm diffusion coefficient can accelerate particles up to the maximum energy $E_{max} \sim 2 \times 10^{14} Z (W_{51}/n)^{2/5}$ [eV], which is reached at the beginning of the Sedov phase of supernova remnant evolution. Until recently, the assumption of the Bohm diffusion coefficient D_{B0} near the shock wave in a supernova remnant was common in the analysis of cosmic ray acceleration (see Ref. [10]).

Recent advances [11–14] in the theory of the strong streaming instability of cosmic rays in a shock wave precursor demonstrate that it is incorrect to use the Bohm acceleration limit in the interstellar field. In particular, it turns out that the stochastic field increases to $\delta B \gg B_0$ for $u_{sh} \gg 10^3$ km s^{-1}, while it rapidly decreases to $\delta B < B_0$ for $u_{sh} < 10^3$ km s^{-1} with the supernova remnant age, due to the dissipation of turbulence. Under extreme conditions, which can apparently occur at the initial phase of supernova shell expansion, the random field can reach the value $\delta B_{max} \sim 10^3 (u_{sh}/3 \times 10^4\ [\text{km s}^{-1}])\, n^{1/2}$ [μG], and the maximum energy of accelerated particles can reach the value $E_{max} \sim 10^{17} Z (u_{sh}/3 \times 10^4\ [\text{km s}^{-1}])^2 M_{ej}^{1/3} n^{1/6}$ [eV] (here, M_{ej} is the discarded shell mass in units of solar masses). The presence of a strong magnetic field is confirmed by observations of nonthermal X-ray emission from young supernova remnants. A large field increase in the young remnants is indirect evidence of proton acceleration accompanied by a strong streaming instability. The dependence $E_{max}(t)$ predicted by the streaming instability theory is stronger than the dependence $E_{max} \sim t^{-1/5}$ obtained under the Bohm diffusion assumption with the coefficient D_{B0}, which allows understanding why the TeV gamma emission is only observed from relatively young supernova remnants. Another consequence of the strong magnetic field is the steepening of the accelerated particle spectrum because of the Alfvén particle drift effect behind the shock wave front (particle drift is caused by Alfvén waves propagating mostly away from the shock wave front), which seems to reconcile the galactic cosmic ray spectrum and the empirical model of cosmic ray origin.

Figure 1 shows the spectrum of cosmic rays in the interstellar medium calculated in Ref. [15]. The proton, helium, and iron spectra are given in the kinetic energy range from 1 GeV per nucleon to 10^3 GeV per nucleon, where reliable data for particular ion types exist, and total spectra of protons and all ions up to iron ions for the energy $E \geqslant 10^3$ GeV per particle. The absolute normalization of various ion sources is done by matching with observed cosmic ray intensities and compositions at the same particle energy 10^3 GeV. The simulations were done using a numerical code that allows modeling the evolution of a spherical shock wave generated by a supernova explosion, and particle acceleration accounting for back reaction of the particle pressure on the hydrodynamic flow. The cosmic ray acceleration is taken into account in type-Ia, IIP, Ib/c, and IIb supernova remnants. Conversion of the supernova explosive kinetic energy into the energy of accelerated cosmic rays becomes efficient at the beginning of the Sedov (adiabatic) phase of the shock wave evolution, i.e., when the supernova outburst mass equals the gas mass 'grabbed' by the shock wave. As a result, a characteristic break — a 'knee' — appears in the particle spectrum averaged over the total time of acceleration by the evolving shock wave. The knee energy is approximately estimated as $p_{knee} c/Z \sim 1 \times 10^{15} W_{51} n^{1/6} M_{ej}^{-2/3}$ [eV]. The calculated spectra agree well with observations up to energies $\sim 5 \times 10^{18}$ eV (this is the maximum energy of iron nuclei accelerated in type-IIb supernova remnants). Owing to summation over all supernova types and various nuclei, the knee is reproduced in the spectra of all particles at the energy 3×10^{15} eV. Overall, approximately 1/3 of the supernova explosion kinetic energy is converted into cosmic rays.

It is assumed in the above calculations that the ultrarelativistic particle diffusion coefficient in the interstellar medium outside the source area depends on the momentum as $D \propto (p/Z)^{0.54}$ in the entire energy range considered [17]. This dependence can actually be established only up to energies of the order of several hundred GeV per nucleon,

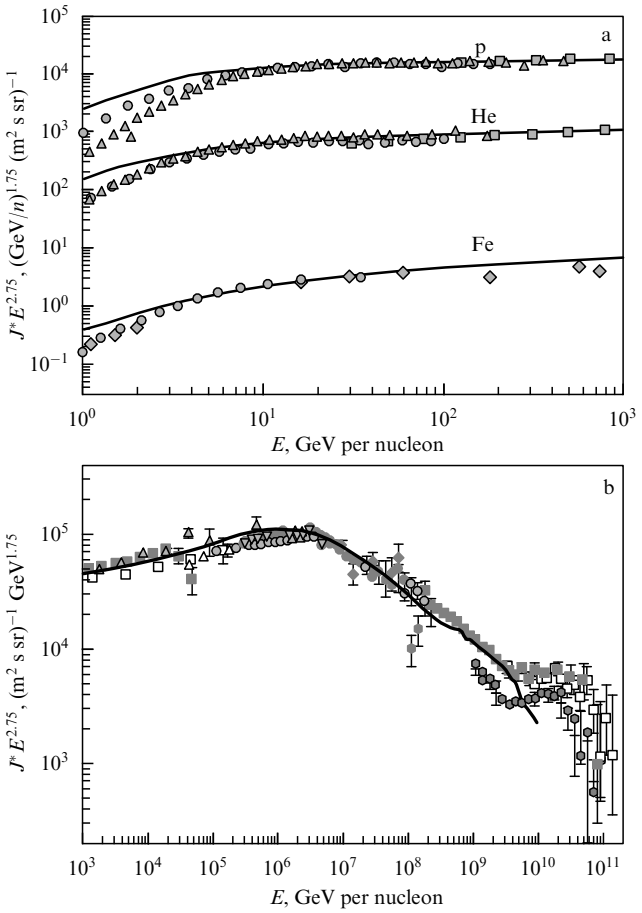

Figure 1. (a) The calculated proton, helium, and iron spectra in the interstellar medium (without the solar wind modulation effect at small energies). Observation data are taken from Ref. [15]. (b) The calculated total spectrum for all particles with energies higher than 10^3 GeV. Observation data are taken from Ref. [16].

for which there are data on the content of secondary nuclei in the cosmic ray composition. (Secondary nuclei such as deuterium, tritium, beryllium, boron, and a number of others are rare in nature; in cosmic rays, they appear as a result of nuclear fragmentation of heavier primary nuclei that traverse the thickness of interstellar matter $\sim 10\ \mathrm{g\ cm^{-2}}$ before leaving the Galaxy.) Physical reasons based on examining particle diffusion in the galactic magnetic fields suggest that the required power-law momentum dependence of the diffusion coefficient extends to energy values of the order of $E/Z \sim 10^{17}$ eV [2]. Refining the cosmic ray propagation features at higher energies requires additional trajectory simulations with various assumptions on the structure of the galactic magnetic field, including the possible presence of the galactic wind with a frozen-in magnetic field and with typical scales of a few hundred kiloparsecs.

Supernova remnants are the main but by no means the only relativistic particle source in the interstellar medium. In particular, pulsars generating high-energy electron–positron pairs can be responsible for the positrons observed in cosmic rays. The measured flux of positrons with energies higher than 10 GeV [18] is stronger than the expected flux of secondary positrons produced in cosmic ray interactions with interstellar gas atoms, and the pulsar contribution explains this contradiction in principal. It is very important to finally clarify the nature of such a high positron flux in cosmic rays because an alternative explanation suggests that these positrons are products of dark matter decay (see the discussion in Refs [19, 20]).

3. Ultrahigh-energy cosmic rays

The core problem for the astrophysics of cosmic rays remains the issue of the origin of particles with ultrahigh energy $E > 10^{19}$ eV. The observed sharp decrease in the particle flux for energies higher than 5×10^{19} eV [21, 22] indicates that these particles interact with the cosmic background radiation photons for more than 3×10^9 years and are of extragalactic origin. Such ultrahigh-energy protons lose energy through electron–positron pair production and pion production (the Greisen–Zatsepin–Kuzmin effect [23, 24]), and the nuclei, in addition, undergo photodecay. Cosmic rays with energies less than 10^{17} eV observed near Earth are of galactic origin and were accelerated in supernova remnants. The characteristic energy value E_c in the range $10^{17}\ \mathrm{eV} < E_c < 10^{19}$ eV, corresponding to the galactic component being changed by the extragalactic one, is debatable [25].

Simple estimates [16, 26, 17] show that from the standpoint of energy balance, jets of active galactic nuclei can be the sources of observed ultrahigh-energy cosmic rays. To maintain the cosmic ray intensity observed at energies higher than 10^{19} eV in the interstellar medium, the source power about $3 \times 10^{36}\ \mathrm{erg\ s^{-1}\ Mpc^{-3}}$ is necessary. This value apparently increases by at least an order in magnitude when the contribution of less energetic particles is taken into account. At the same time, jets of active galactic nuclei release kinetic energy of the order of $10^{40}\ \mathrm{erg\ s^{-1}\ Mpc^{-3}}$, and approximately 2% of this energy is in jets with the power $L_{\mathrm{jet}} = 10^{44} - 10^{46}\ \mathrm{erg\ s^{-1}}$, which is typical for radio galaxies and quasars with large radio luminosity. The value $L_{\mathrm{jet}} = 10^{40} - 10^{44}\ \mathrm{erg\ s^{-1}}$ is characteristic for numerous less powerful jets.

Without detailing the cosmic ray acceleration mechanism in jets, the Hillas criterion [28] can be used to estimate the maximum energy $E_{\max}$ that particles with the charge Ze can acquire in an acceleration region of size l, with the magnetic field B, and the magnetic field transfer velocity $u = \beta c$: $E_{\max} = Ze\beta Bl$. We note that this estimate is valid up to a numerical factor, for example, in the case of particle diffusion acceleration on a shock wave front in a supernova remnant by assuming the Bohm diffusion in the field B for energetic particles near the shock wave front. To estimate the magnetic field, we assume that the energy flux of the frozen statistically isotropic magnetic field in the jet is related to the kinetic energy flux as $L_{\mathrm{jet}} = \beta c(B^2/6\pi)\pi R^2$, where $R = l/2$ is the jet cross section and βc is its velocity. As a result, we obtain the following estimate for the maximum possible energy of accelerated particles [29–32]:

$$E_{\max} = Ze\left(\frac{6\beta}{c}\, L_{\mathrm{jet}}\right)^{1/2} \approx 2.7 \times 10^{20} Z\beta^{1/2} L_{\mathrm{jet},45}^{1/2}\ [\mathrm{eV}]\,,$$

where the notation $L_{\mathrm{jet},45} = L_{\mathrm{jet}}[(10^{45}\ \mathrm{erg\ s^{-1}})^{-1}]$ is used. The maximum detected energy of cosmic ray events is approximately 2×10^{20} eV.

The above estimates demonstrate that according to general energy characteristics and the maximum possible energy value of accelerated particles, jets of galaxies with active nuclei can be the main sources of the highest-energy cosmic rays observed. More detailed discussions can be found in reviews [16, 27].

References

1. Ginzburg V L, Syrovatskii S I *Proiskhozhdenie Kosmicheskikh Luchei* (The Origin of Cosmic Rays) (Moscow: Izd. AN SSSR, 1963) [Translated into English (Oxford: Pergamon Press, 1964)]
2. Ginzburg V L (Ed.) *Astrofizika Kosmicheskikh Luchei* (Astrophysics of Cosmic Rays) (Moscow: Nauka, 1990); 2nd ed. (Moscow: Nauka, 1990) [Translated into English (Amsterdam: North-Holland, 1990)]
3. Lozinskaya T A *Sverkhnovye Zvezdy i Zvezdnyi Veter*: *Vzaimodeistvie s Gazom Galaktiki* (Supernovae and Stellar Wind in the Interstellar Medium) (Moscow: Nauka, 1986) [Translated into English (New York: AIP, 1992)]
4. Vink J *Adv. Space Res.* **33** 356 (2004)
5. Aharonian F et al. *Astrophys. J.* **636** 777 (2006)
6. *Space Sci. Rev.* **99** (1–4) (2001)
7. Krymskii G F *Dokl. Akad. Nauk SSSR* **234** 1306 (1977) [*Sov. Phys. Dokl.* **22** 327 (1977)]
8. Bell A R *Mon. Not. R. Astron. Soc.* **182** 147 (1978)
9. Berezhko E G *Adv. Space Res.* **41** 429 (2008)
10. Berezhko E G, Elshin V K, Ksenofontov L T *Zh. Eksp. Teor. Fiz.* **109** 3 (1996) [*JETP* **82** 1 (1996)]
11. Bell A R, Lucek S G *Mon. Not. R. Astron. Soc.* **321** 433 (2001)
12. Ptuskin V S, Zirakashvili V N *Astron. Astrophys.* **403** 1 (2003)
13. Bell A R *Mon. Not. R. Astron. Soc.* **353** 550 (2004)
14. Zirakashvili V N, Ptuskin V S *Astrophys. J.* **678** 939 (2008)
15. Ptuskin V S, Zirakashvili V N, Seo E-S *Astrophys. J.* **718** 31 (2010)
16. Blümer J, Engel R, Hörandel J R *Prog. Part. Nucl. Phys.* **63** 293 (2009)
17. Jones F C et al. *Astrophys. J.* **547** 264 (2001)
18. Adriani O et al. *Nature* **458** 607 (2009)
19. Profumo S, arXiv:0812.4457
20. Katz B et al. *Mon. Not. R. Astron. Soc.* **405** 1458 (2010)
21. Abbasi R U et al. (High Resolution Fly's Eye Collab.) *Phys. Rev. Lett.* **100** 101101 (2008)
22. Abraham J et al. (The Pierre Auger Collab.) *Phys. Rev. Lett.* **101** 061101 (2008)
23. Greisen K *Phys. Rev. Lett.* **16** 748 (1966)
24. Zatsepin G T, Kuz'min V A *Pis'ma Zh. Eksp. Teor. Fiz.* **4** 114 (1966) [*JETP Lett.* **4** 78 (1966)]
25. Aloisio R et al. *Astropart. Phys.* **27** 76 (2007)
26. Torres D F, Anchordoqui L A *Rep. Prog. Phys.* **67** 1663 (2004)
27. Sigl G *New J. Phys.* **11** 065014 (2009)
28. Hillas A M *Annu. Rev. Astron. Astrophys.* **22** 425 (1984)
29. Lovelace R V E *Nature* **262** 649 (1976)
30. Blandford R D *Phys. Scripta* **T85** 191 (2000)
31. Waxman E *New J. Phys.* **6** 140 (2004)
32. Farrar G R, Gruzinov A *Astrophys. J.* **693** 329 (2009)